IJMMM International Journal of Minerals, Metallurgy and Materials 矿物冶金与材料学报（英文版）

Recent progress in constructing fluorinated solid–electrolyte interphases for stable lithium metal anodes

Di Zhang, Pengfei Lv, Wei Qin, Xin He, and Yuanhua He

Cite this article as:
Di Zhang, Pengfei Lv, Wei Qin, Xin He, and Yuanhua He, Recent progress in constructing fluorinated solid–electrolyte interphases for stable lithium metal anodes, *Int. J. Miner. Metall. Mater.*, 32(2025), No. 2, pp. 270-291. https://doi.org/10.1007/s12613-024-2996-3

INTERNATIONAL JOURNAL OF
Minerals, Metallurgy and Materials

Volume 32, Number 2, February 2025
Page 270

Review

https://doi.org/10.1007/s12613-024-2996-3

Recent progress in constructing fluorinated solid–electrolyte interphases for stable lithium metal anodes

Di Zhang[1)], *Pengfei Lv*[1)], *Wei Qin*[1)], *Xin He*[2),✉], *and Yuanhua He*[1),✉]

1) Civil Aircraft Fire Science and Safety Engineering Key Laboratory of Sichuan Province, College of Civil Aviation Safety Engineering, Civil Aviation Flight University of China, Guanghan 618307, China

2) School of Chemical Engineering, Sichuan University, Chengdu 610065, China

(Received: 3 April 2024; revised: 25 August 2024; accepted: 27 August 2024)

Abstract: Lithium metal batteries (LMBs) are emerging as a promising energy storage solution owing to their high energy density and specific capacity. However, the non-uniform plating of lithium and the potential rupture of the solid–electrolyte interphase (SEI) during extended cycling use may result in dendrite growth, which can penetrate the separator and pose significant short-circuit risks. Forming a stable SEI is essential for the long-term operation of the batteries. Fluorine-rich SEI has garnered significant attention for its ability to effectively passivate electrodes, regulate lithium deposition, and inhibit electrolyte corrosion. Understanding the structural components and preparation methods of existing fluorinated SEI is crucial for optimizing lithium metal anode performance. This paper reviews the research on optimizing LiF passivation interfaces to protect lithium metal anodes. It focuses on four types of compositions in fluorinated SEI that work synergistically to enhance SEI performance. For instance, combining compounds with LiF can further enhance the mechanical strength and ionic conductivity of the SEI. Integrating metals with LiF significantly improves electrochemical performance at the SEI/anode interface, with a necessary focus on reducing electron tunneling risks. Additionally, incorporating polymers with LiF offers balanced improvements in interfacial toughness and ionic conductivity, though maintaining structural stability over long cycles remains a critical area for future research. Although alloys combined with LiF increase surface energy and lithium affinity, challenges such as dendrite growth and volume expansion persist. In summary, this paper emphasizes the crucial role of interfacial structures in LMBs and offers comprehensive guidance for future design and development efforts in battery technology.

Keywords: LiF; lithium metal anodes; solid–electrolyte interphase; interface; cycling stability

1. Introduction

Lithium metal batteries (LMBs) are attracting attention for their potential to deliver higher voltage and energy density compared to conventional lithium-ion batteries (LIBs). This advantage is largely owing to lithium metal's ultrahigh specific capacity and its position as the lowest electrochemical potential. While LIBs have revolutionized portable devices and electric vehicles, their energy density, typically around 250 $Wh \cdot kg^{-1}$ [1], still falls short of eliminating concerns about driving range and device endurance. To address these limitations, researchers are replacing traditional graphite-based intercalation anodes with metallic lithium (Li) to form LMBs. This includes solid-state batteries metal/air or lithium/sulfur batteries, which are widely seen as promising candidates expected to outperform LIBs in both energy density and specific energy [2]. Theoretically, LMBs with Li metal anode (LMA) and layered oxide cathode can achieve an energy density of 400 $Wh \cdot kg^{-1}$, making them a strong candidate for powering electric vehicles. However, this technology is very complex and has various drawbacks, such as poor rate capability, electrolyte decomposition, and the formation of reactive intermediates during charging.

Nevertheless, LMBs face significant challenges that hinder their practical feasibility. Li metal is highly reactive, both chemically and electrochemically, with nearly all electrolyte parts like solvents, additives, and Li salts. This reactivity stems from its ultralow electrochemical potential (−3.04 V vs. SHE (standard hydrogen electrode)). These side reactions produce byproducts that result in a solid–electrolyte interphase (SEI) on the LMA surface [3]. During electrochemical deposition, heterogeneous SEI can cause uneven development of Li deposits, commonly referred to as "dendrites". These dendrites, which appear in different structures, such as needle-like, mossy, or granular deposits [4], result from ionic conductivity. Along with the stripping and plating processes, this heterogeneous deposition and incomplete Li dissolution lead to significant volume changes in the LMA. This not only destroys the native SEI but also exposes fresh, highly reactive Li surfaces to the electrolyte. The repeated rupture and reforming of the SEI all dendrites to grow erratically, leading to the accumulation of inactive Li [5–6]. The issues of uneven

✉ Corresponding authors: Xin He E-mail: xinhe@scu.edu.cn; Yuanhua He E-mail: heyuanhua@cafuc.edu.cn

metal deposition, interfacial side reactions forming SEI, and severe volume expansion of the Li cathode are primary causes of hindered Li^+ transport, shortened battery cycle life, reduced Coulomb efficiency (CE), capacity decay, and rapid battery failure [6–7].

As characterization techniques continue to advance rapidly, several studies have investigated the failure mechanisms of LMAs and proposed feasible solutions. These included innovations such as liquid electrolyte engineering to change interfacial components and morphology to improve the cathode CE [8], the use of inorganic solid electrolytes with high Li^+ conductivities to replace flammable traditional organic liquid electrolytes [9–11], three-dimensional (3D) materials that provide a framework for metal deposition, mitigating volume changes in Li [12], and modification of the Li metal surface to improve native SEI defects. Research in interface engineering is increasingly prioritized in both industry and academia owing to its effectiveness in performance improvement, wide applicability, and importantly, the ability to precisely control various battery performance aspects. This approach addresses almost all of the abovementioned problems faced by LMAs through the judicious design and tuning of the chemical and physical properties of the interface. Therefore, high-performance SEI is advancing safe, high energy density, and stable metal anodes.

In recent years, the critical role of SEI for battery stability has been widely recognized, unveiling its intrinsic mechanisms and functions to guide future research. In 1979, Peled's classical study highlighted an ultrathin film formed at the interface between LMA and an electrolyte, identifying an interfacial layer with both barrier and protective properties [13]. This led to the proposal of the double-layer structure model, which assumes that side reactions at the Li metal surface proceed gradually. Initially, intermediate products form in the electrolyte before diffusing to the LMA for further transformation. Consequently, a thin, dense inorganic layer and a thick, porous organic outer layer, composed mainly of salts like Li_2O, Li_3N, LiF, and Li_2CO_3, develop near the Li metal surface [13]. Recent studies using molecular dynamics simulations and liquid secondary-ion mass spectrometry have confirmed the consistency of this structure with the "double-layer structure model" [14]. In 1985, the presence of both organic outer layer and inorganic inner layer was confirmed through *in situ* X-ray diffraction (XRD) [15]. Soon afterward, X-ray photoelectron spectroscopy (XPS) clarified that Li_2CO_3 is a main component of the inorganic inner layer [16]. In 1997, based on these characterization results, Peled optimized the double-layer structure model and introduced the mosaic model, which better represents the SEI structure when produced by LMA and graphite anode. This model suggests that interfacial components form directly on the Li metal surface without the intermediate product transformation. Therefore, the SEI consists of outer layer of organic oligomers and inner layer of inorganic products adjacent to the Li metal surface. To better understand and describe the SEI structure, researchers proposed additional models such as the "polymer electrolyte interphase" [17], "solid polymer layer" [18], and "compact stratified layer" [19].

Researchers can determine the basic components of the SEI by examining the solvent and salt composition in the electrolyte. For example, LiF components are commonly detected in fluorine (F)-containing electrolytes such as tetrafluoroborate (BF_4^-) [20], hexafluorophosphate (PF_6^-) [21], and fluoroethylene carbonate (FEC) [22]. Despite their potential, SEI exhibits a complex internal structure owing to their composition, structure, and mechanical properties, which vary depending on the electrolyte, charge state, temperature, and other factors. F components play a key role in both liquid- and solid-state battery systems, with Li halides, especially LiF, increasingly becoming the main components of passivated interphases [23–25]. Investigation into the artificial SEIs' composition has shown that adding compounds such as LiF and other vinyl chloride (VC) to Li foil enhances the ionic conductivity and structural stability of these interfaces [26]. Fluorinated SEIs are known for their mechanical stability, high interfacial energy, and excellent electronic insulation, which can prevent electrolyte erosion on LMA, inhibit dendrite growth, and promote homogeneous Li deposition [13,24,27–28]. In addition to fluorinated SEI, various materials such as Al_2O_3, carbon materials, diamond, 2D materials, and organic polymers have been reported. Although the Al_2O_3 layer shields the anode from electrolyte reactions, electron tunneling remains a challenge. Carbon materials are commonly used to protect LMAs and provide sites for the orderly deposition of Li, and diamonds offer higher rigidity for artificial SEIs. However, these materials often struggle to maintain interface stability at high charge/discharge rates. Two-dimensional materials, widely prized for their unique planar structure, face production challenges owing to complicated processes and low controllability. Organic polymer artificial SEIs provide flexibility and adaptability during Li deposition/stripping but lack the mechanical strength to inhibit dendrite growth over prolonged use. Fluorinated SEIs serve as effective passivation layers, preventing electron tunneling and promoting homogeneous Li plating, thus improving the lifespan and interfacial stability of LMAs during repeated Li stripping and plating [29]. These findings provide a foundation for developing higher-quality artificial SEIs on Li metal surface.

The mechanisms of various functional LiF-rich hybridized SEIs and the protective impact of the LiF passivation layer on Li metal have garnered increased attention owing to research highlighting the beneficial properties of LiF. Various approaches have been proposed for preparing pure LiF coatings on Li metal surface and multifunctional LiF-rich hybridized SEIs. This review begins by introducing the structure of the F-rich interphase and elucidates the mechanisms through which LiF affects the interface, notably in terms of Li diffusion and deposition. We then summarize recent progress in stabilizing LMAs with pure LiF coatings and LiF-rich SEIs prepared by various methods. Finally, we discuss the multifaceted effects of F-rich composite SEIs obtained by

hybridizing LiF with materials of different characteristics, including compounds, polymers, metals, and alloys. We also provide insights into future developments in F-rich interphases (Fig. 1).

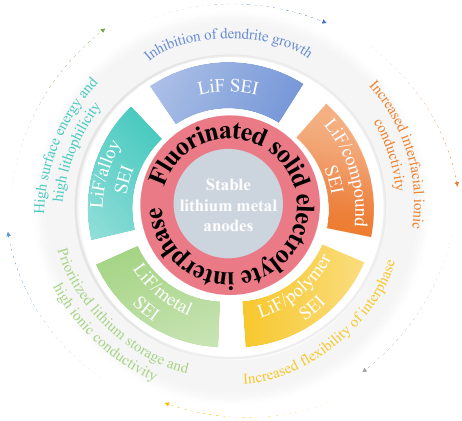

Fig. 1. Schematic of the representative strategies for achieving stable LMAs using constructing fluorinated SEIs.

2. Characteristics of fluorine-rich solid–electrolyte interphases

As the primary constituent of the mosaic inorganic layer of SEIs, LiF is the most stable alkali metal fluoride. This compound forms spontaneously when Li interacts with organic electrolytes, primarily derived from the *in situ* chemical and electrochemical decomposition products of Li salts and fluoride in the electrolyte. It is an essential component of LMBs and is responsible for homogenizing Li deposition and controlling Li diffusion. The LiF-rich layer controls the homogeneous stripping and plating of Li during battery cycles. This is attributed to its optimal diffusion barrier, reduced ionic conductivity (ranging from 10^{-10} to 10^{-8} S·cm^{-1} at ambient temperature), enhanced surface energy, and high mechanical modulus.

Although LiF's ionic conductivity is lower compared to other solid–electrolyte materials, such as Li_2CO_3 (~10^{-8} S·cm^{-1}) [30], it provides a less favorable environment for Li^+ diffusion and transport. Nevertheless, LiF possesses a broad electrochemical stability window [30–31], which hinders the diffusion and transport of Li^+. However, LiF possesses a broad electrochemical stability window (ranging from 0 to 6.4 V vs. Li), negligible solubility in most electrolytes [32], and relatively low surface diffusion barriers when compared to non-halide SEI materials. These attributes ensure effective isolation of the electrolyte from the Li metal, preventing negative interactions with organic electrolytes that could impair transport kinetics and lead to irreversible electrolyte consumption. The binding site for F^- adatom is directly above the ion ("anion site"). In its transition state of diffusion, the adatom is located between two anions and the two cations ("in-between site"). The higher amount of electron transfer at the LiF(001)/Li(001) interface indicates stronger interfacial bonding strength, thus indicating a stronger stability (Fig. 2(a)) [33]. The diffusion barrier, equal to the energy difference between the binding and transition sites, is critical in enhancing Li^+ transport [34]. Strong Li–F bond interactions improve the short-range cation arrangement at the interface, leading to a relatively homogeneous planar deposition of Li under the SEI layer.

LiF performs relatively poorly compared with Li_2CO_3 in terms of interfacial mechanical stability [35]. However, density functional theory computations offer a thorough comparison of the mechanical and electrochemical characteristics of the two significant interphases, LiF/Li and Li_2CO_3/Li. During charging cycles, Li^+ is highly susceptible to nucleation and growth at the Li_2CO_3/Li interphase. By contrast, LiF presents a higher electron tunneling barrier, restricting elec-

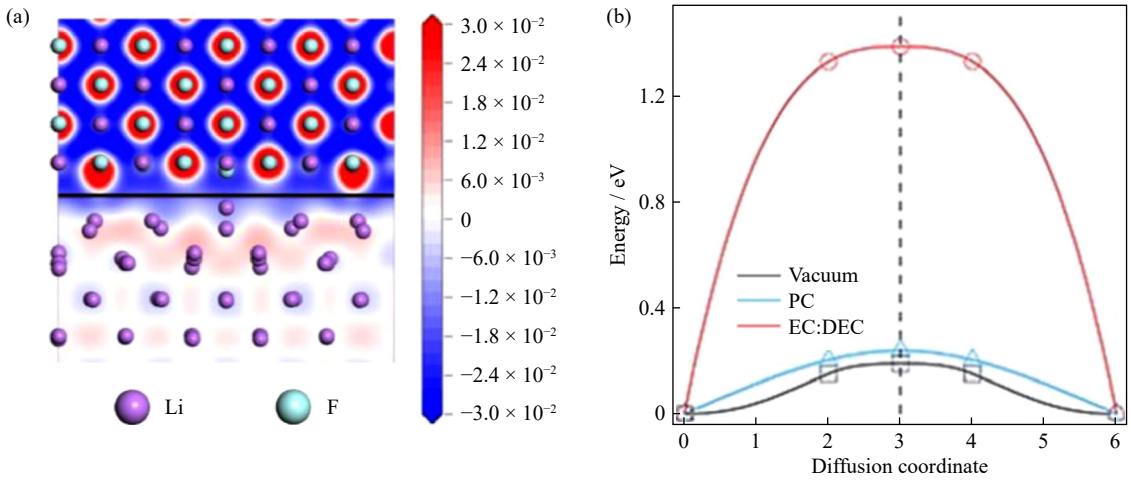

Fig. 2. (a) Charge distribution of LiF(001)/Li(001) interface and (b) acquired energies of nudged elastic band (NEB) images varying with the diffusion coordinates in vacuum, ethylene carbonate (EC)/diethyl carbonate (DEC), and propylene carbonate (PC) electrolytes. (a) Reprinted from *Surf. Interfaces*, 44, Y. Xu, Y.W. Sun, Y. Sun, H.Y. Fang, Y. Jiang, and B. Zhao, Theoretical calculation study on the electrochemical properties of lithium halide-based artificial SEI films for lithium metal anodes, 103768, Copyright 2024, with permission from Elsevier. (b) Republished with permission of Royal Society of Chemistry, from Regulating Li deposition at artificial solid electrolyte interphases, L. Fan, H.L. Zhuang, L.N. Gao, Y.Y. Lu, and L.A. Archer, 5, 2017; permission conveyed through Copyright Clearance Center, Inc.

tron transport to the electrolyte, thereby limiting electron tunneling in the LiF/Li interphase [35]. Despite its reduced diffusion potential barrier, LiF's surface energy is comparable to or higher than that of Li_2CO_3. Climbing-image nudged elastic band (CI-NEB) calculations indicate that in a vacuum and EC/DEC and (PC) electrolytes, Li atoms must overcome energy barriers of 0.19, 1.38, and 0.24 eV, respectively to diffuse between the two atoms of F on the LiF surface (001) (Fig. 2(b)). Using joint density flooding theory (DFT), Lu *et al*. [11] demonstrated that the presence of halide anions, particularly fluorine, enhances the surface diffusion coefficient of Li in the electrolyte/LMA interphase. This facilitates smoother and more efficient Li^+ diffusion, promoting dendrite-free Li metal deposition, thus prolonging the cycle stability and lifespan of LMBs. Therefore, LiF-rich passivation interphases are important for Li metal deposition.

3. Construction of LiF solid–electrolyte interphases

To harness the excellent characteristics of LiF as an interfacial protection material, many strategies have been proposed to increase the F content in SEI layers. A key focus of research is the creation of high-quality, continuous LiF coatings for uniform Li deposition. The classical approach involves the fluorination of Li using gases. Initially, Lin *et al*. [32] formed a conformal LiF coating on 3D layered Li composite electrode by reacting Li foil *in situ* with commercial Freon R134a gas (Fig. 3(a)). This process was conducted in a specially sealed vessel with optimized conditions set at 50.6625 kPa pressure and 150°C for forming high-quality LiF coatings. Even at a high charge rate (2 C), lithium–sulfur (Li–S) batteries with LiF coating sustained a high capacity of 800 $mAh \cdot g^{-1}$), demonstrating that a decrease in negative po-

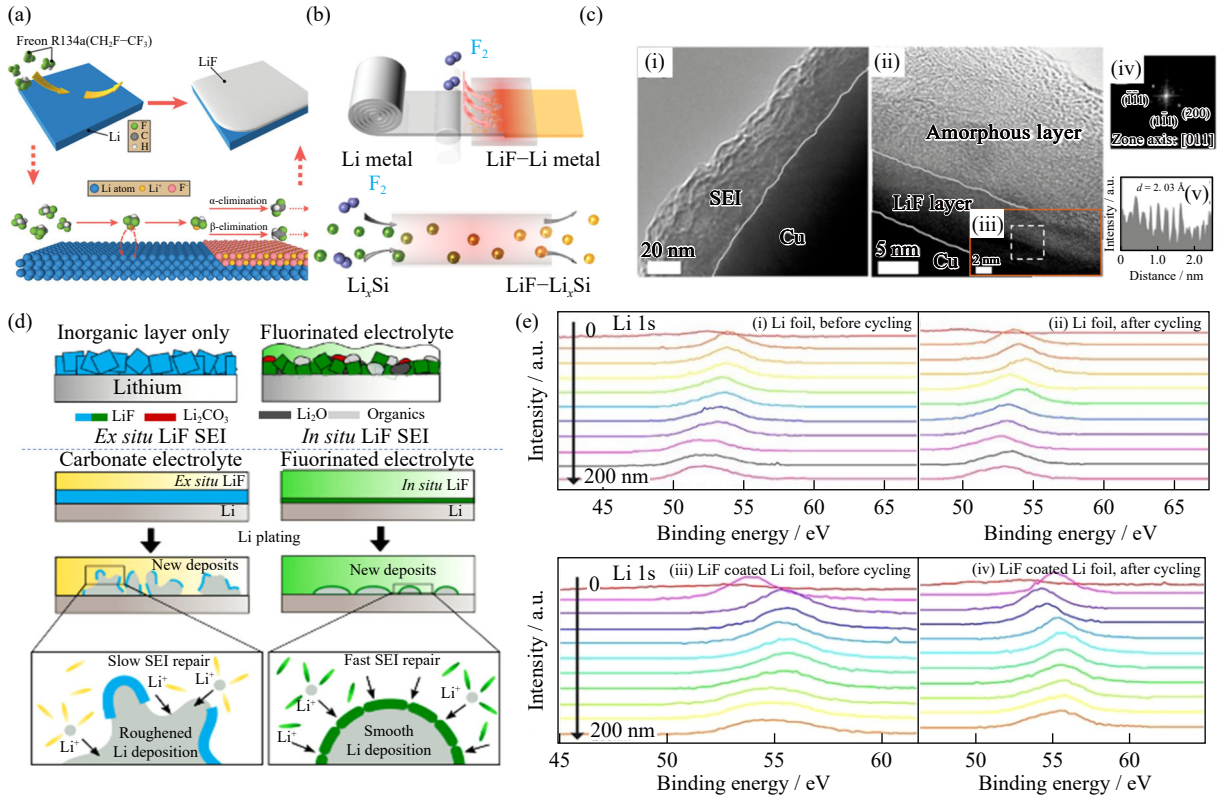

Fig. 3. (a) Diagram illustrating the surface modification of Li using Freon R134a and key chemical reactions at the initial phase, where an intermediate (CH_2F–CF_2)–Li^+ can be produced, subsequently leading to either α or β elimination. (b) Illustration of surface fluorination of Li metal and pre-lithiated Si anodes. Upon heating, the fluoropolymer CYTOP gradually decomposes, liberating pure F_2 gas. This F_2 gas then interacts with either Li metal or Li_xSi NPs, forming a homogenous and compact LiF deposition. (c-(i–iii)) STEM and magnified image of the *in situ* LiF SEI formed by plating/stripping Li on Cu TEM grid. (c-iv) Fast Fourier transformation pattern and (c-v) intensity plot of the dashed region in (c-iii). (d) Varying structures (top) of the *ex situ* LiF-enriched SEI from non-electrolytic F sources (left) and the *in situ* LiF-enriched SEI from F-rich electrolytes (right) on Li; Li deposition (bottom) with an *ex situ* LiF SEI in carbonate electrolyte (left), and an *in situ* LiF SEI in the fluorinated electrolyte (right). (e) XPS analysis of the surface film on the Li metal electrode. Li signals of bare Li foil (i) before and (ii) after cycling, and Li signals of LiF-coated Li foil (iii) before and (iv) after cycling (Depth profiles are all arranged from top to a depth of 200 nm with an increment of 20 nm). (a) Reprinted with permission from D.C. Lin, Y.Y. Liu, W. Chen, *et al*., *Nano Lett*., 17, 3731-3737 (2017) [32]. Copyright 2017 American Chemical Society. (b) Reprinted with permission from J. Zhao, L. Liao, F.F. Shi, *et al*., *J. Am. Chem. Soc*., 139, 11550-11558 (2017) [25]. Copyright 2017 American Chemical Society. (c, d) M.F. He, R. Guo, G.M. Hobold, H.N. Gao, and B.M. Gallant, Proc. *Natl. Acad. Sci*., 117, 73-79, 2020. (e) Republished with permission of Royal Society of Chemistry, from Regulating Li deposition at artificial solid electrolyte interphases, L. Fan, H.L. Zhuang, L.N. Gao, Y.Y. Lu, and L.A. Archer, 5, 2017; permission conveyed through Copyright Clearance Center, Inc.

larization enhanced active surface and uniform ion flux of the LiF coating. Similarly, Zhao *et al*. [25] proposed a representative and instructive method for the *ex situ* reaction with F-containing gases (Fig. 3(b)). They utilized fluoropolymer CYTOP as a safe, solid source. Upon decomposition, CYTOP progressively releases pure fluorine gas at 175°C over 12 h, which then reacts with LMA to form a consistent and compact LiF coating [25]. The inert LiF-rich interphases functioned as stable interfacial layers on the LMA, mitigating electrolyte corrosion and preventing dendrite development. The LiF–Li electrode remained stable over 300 cycles at a high current density of 5.0 $mA \cdot cm^{-2}$ without dendrite development. He *et al*. [36] introduced a novel approach using NF_3 gas as a reactant. This method minimizes contamination during the reaction. By increasing the ambient temperature, they enhanced the *ex situ* reaction between Li and NF_3, achieving only a 1.5% fluorine atom concentration after 16 h of reaction at room temperature. Similar to other reported artificial LiF layers [25,31,33,37], the obtained samples showed minimal contamination from common elements such as C, which are usually present in other LiF synthesis methods [25,37]. In studies comparing *in situ* and *ex situ* generated SEI layers, notable differences in overpotential stability were observed. The *in situ* SEI generated in fluorinated electrolytes exhibited lower and more stable overpotential over 80 cycles compared to the *ex situ* LiF layers formed in carbonate electrolytes. This difference can be attributed to their distinct microscopic morphologies, as revealed by scanning transmission electron microscopy (STEM) (Fig. 3(c)). The *in situ* LiF SEI consists of single LiF crystal, featuring a crystalline inner layer approximately 8 nm thick and an amorphous outer layer. Conversely, the *ex situ* LiF artificial SEI, formed through reactions between Li and the electrolyte, gradually became thick and porous owing to slow repair processes in the carbonate electrolyte environment (Fig. 3(d)). Further insights were gained through another study that conducted deep etching X-ray photoelectron spectroscopy (XPS) analysis of the LiF SEI before and after cycling (Fig. 3(e)). The binding energy of the LiF-coated Li anode remained stable at 56 eV before and after cycling. By contrast, the binding energy of the lithium peak on a bare lithium anode shifted from 55 to 52 eV as it cycled, indicating a movement from the second layer to the last layer, with a weakening LiF signal. This also indicates the stable existence of the LiF artificial protective layer [31].

Many effective electrolyte additives such as FEC, HF, fluorinated compounds, and highly concentrated electrolytes have been proposed in recent studies to improve battery performance. For example, a high concentration of 6 M Li bis(fluorosulfonyl)imide (LiFSI) in 1,2-dimethoxyethane (DME) (~20 μL) infiltrated the space between Li_3PS_4 (LPS) solid-state electrolyte (SSE) and the LMA [38]. This setup resulted in a thin, homogeneous LiF-rich SEI layer that efficiently suppressed and prevented undesired reactions between Li and LPS. The LiF-rich SEI coating provided enhanced interfacial energy (γ), a high shear modulus, and low electronic conductivity. Because of LiF's lower Li^+ diffusion energy barrier than Li_2CO_3, as well as its low resistance in close contact with Li and LPS, the thin LiF-rich SEI layer that was produced *in situ* did not decrease ion transport kinetics. The incorporation of LiF additives into electrolytes has proven highly effective in stabilizing the SEI and ensuring uniform Li deposition [11]. Owing to its exceptional impact and low cost, the *in situ* creation of SEIs is considered one of the most practical and successful methods to impede Li dendrite growth. This approach has been widely applied, especially in industrial battery manufacturing. However, continuous consumption of functional additives and Li salts during plating/stripping cycles leads to inevitable changes in the SEI structure. Therefore, chemical or physical *ex situ* fabrication methods for creating artificial SEI preparation have been widely proposed. For example, a common method for preparing LiF-rich layers involves treating Li with specific solutions. Rather than immersing Li fully in a precursor solution, a small amount of an NH_4HF_2-treatment solution can be applied directly to Li. This method, as demonstrated by Yuan *et al*. [39], results in a LiF-rich layer (TPL) film having a decreased thickness of 6.86 μm and particle diameters ranging from 22 to 52.4 nm (Fig. 4(a)). XRD analysis shows peaks at 36.9° and 65.3° are assigned to the crystalline nature of the LiF particles and the TPL component not contaminated by air, respectively (Fig. 4(b)). The porous TPL layer exhibits a high Li storage capacity, allowing TPL-modified cells to sustain stable cycling over 100 cycles at a high current density of 6 $mA \cdot cm^{-2}$. Practically, the protecting LiF layer shields Li against corrosion, ensuring the CE of the Li|LFP complete cell remains above 99% even after 100 cycles at 2 C.

Achieving high-quality continuous LiF coatings on LMA presents challenges. Conventional methods often result in diffuse LiF domains and microcrystalline structures with numerous weakly connected grain boundaries. These imperfections are susceptible to fracture during Li plating and stripping, leading to the fragmentation of the artificially fluorinated SEI structure. To address these issues, the atomic layer deposition (ALD) has been proposed for the direct deposition of high-purity LiF films onto Li metal. This technique operates at reduced temperatures to get highly conformal, uniform, and stoichiometric LiF coatings using lithium tert-butoxide (LiO^tBu) and HF/pyridine (Fig. 4(c)) [37]. Selected area electron diffraction (SAED) images of approximately 15 nm LiF films deposited on silica nanoparticles dispersed on a TEM transmission grid revealed four rings corresponding to the (111), (200), (220), and (311) planes of LiF. Further measurements of the grazing incidence wide-angle X-ray diffraction (GIWAXS) intensity versus q ($Å^{-1}$) (Fig. 4(d)) revealed two broad peaks at 2.78 and 3.21 $Å^{-1}$ corresponding to the (111) and (200) LiF reflections, respectively, and corroborated with the brightest ring in the SAED image. The calculated LiF lattice constant of (3.95 ± 0.03) Å indicates the presence of compressive strain in LiF, with the preferred crystallographic planes being (111) and (220). It is theorized that coatings with a shear modulus twice that of Li can effect-

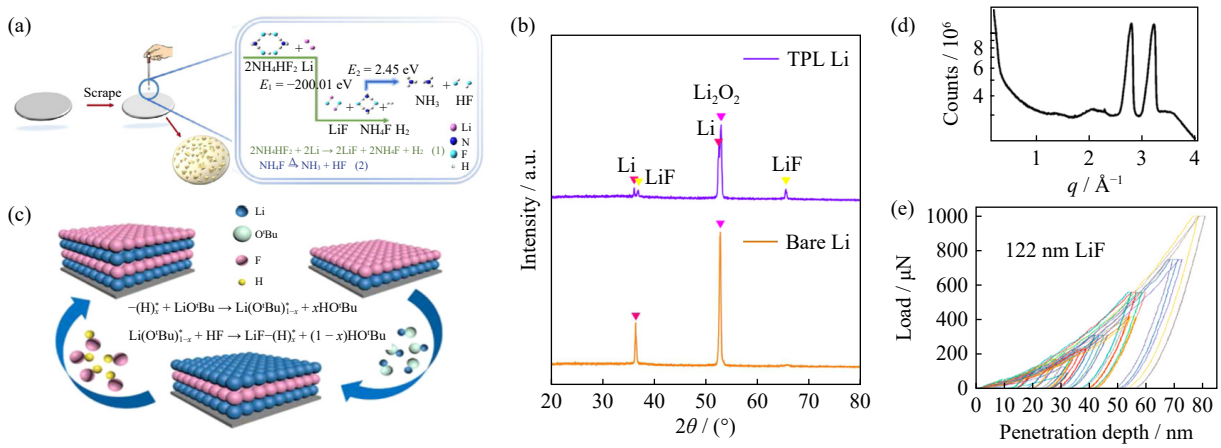

Fig. 4. (a) Diagram showing the preparation procedure of TPL Li and feasibility verification of the chemical reaction at room temperature. (b) XRD patterns of TPL Li and bare Li. (c) Synthesis schematic for atomic layer deposition LiF using LiO^{t}Bu and HF/pyridine. (d) GIWAXS measurement of a 118-nm LiF film on silicon showing the (111) and (200) peaks of the cubic LiF phase. (e) Force–distance curves for a 122-nm LiF film on silicon measured using nanoindentation. (a, b) Reprinted from *J. Energy Chem.*, 37, Y.X. Yuan, F. Wu, G.H. Chen, Y. Bai, and C. Wu, Porous LiF layer fabricated by a facile chemical method toward dendrite-free lithium metal anode, 197-203, Copyright 2019, with permission from Elsevier. (c–e) Reprinted with permission from L. Chen, K.S. Chen, X.J. Chen, *et al.*, *ACS Appl. Mater. Interfaces*, 10, 26972-26981 (2018) [37]. Copyright 2018 American Chemical Society.

ively inhibit dendrite formation [40], and simulations have shown that a coating shear modulus greater than 8.5 GPa is sufficient to inhibit Li dendrite formation [41]. The LiF films prepared through ALD attained a shear modulus of 58 GPa owing to their ultrahigh purity exceeding 99% (Fig. 4(e)), which is sevenfold greater compared to the value necessary to inhibit Li dendrite formation. Subsequently, similar physical deposition techniques have been explored for passivating Li surfaces. For example, Liu *et al.* [29] employed a magnetron sputtering system to thermally evaporate LiF protective layer. This homogeneous layer is crucial for ensuring a uniform flow of Li^+ and facilitating quick Li^+ transport. The layer nanoslits enable the electrolyte to penetrate, offering a sufficiently large number of channels for Li^+ transport. The voltage–capacity curves featuring a Li@LiF anode exhibited almost constant voltage hysteresis, indicating stable interfacial properties. Ko and Yoon [42] investigated the optimal thickness of LiF coatings by thermally evaporating LiF onto Li foil. The findings revealed that a 300-nm LiF-coated Li cell maintained a nearly constant impedance of 69 Ω for 12 h and displayed the most stable overvoltage for 200 h compared to those of other cells with different coating thicknesses (100 and 200 nm). Conversely, the impedance of an uncoated Li cell increased from 77 to 95 Ω over 12 h. The LiF coating protected the Li metal surface, minimizing additional SEI formation and suppressing Li^+ kinetic barriers caused by dendrite growth on bare Li. In summary, both *in situ* and *ex situ* LiF formation on anodes greatly enhanced the electrochemical performance. The optimized electrochemical characteristics of these LiF layers are compiled in Table 1.

Table 1. Summary of the electrochemical performance parameters obtained for LiF SEI layers in symmetric Li|Li cells

Method of preparation	Testing condition	Cycling lifespan	Ref.
In situ gas-phase + reaction between Li metal and gaseous Freon R134a	1 mA·cm^{-2}, 1 mAh·cm^{-2}	450 h	[32]
In situ gas-phase + 6 M LiFSI/DME (~20 μL)	0.3 mA·cm^{-2}	350 cycles	[38]
In situ liquid-phase + 1 M (0.7LiTFSI + 0.3LiF)–PC	0.38 mA·cm^{-2}	1800 h	[11]
In situ liquid-phase + reaction of a small amount of Li metal and NH_4HF_2	2 mA·cm^{-2}, 1 mAh·cm^{-2}	350 h	[39]
Ex situ gas-phase + heating CYTOP to release pure F_2	1 mA·cm^{-2}	300 cycles	[25]
	3 mA·cm^{-2}, 1 mAh·cm^{-2}	180 cycles	
	5 mA·cm^{-2}, 1 mAh·cm^{-2}	300 cycles	
Ex situ gas-phase + reaction between NF_3 gas and Li metal (1 M LiTFSI in DOL/DME (*V*/*V* = 1/1) + 1wt% $LiNO_3$)	0.2 mA·cm^{-2}, 1 mAh·cm^{-2}	1200 h	[36]
Ex situ physical deposition + ALD LiF	1 mA·cm^{-2}, 1 mAh·cm^{-2}	260 h	[37]
Ex situ physical deposition + vacuum evaporation of LiF	1 mA·cm^{-2}, 1 mAh·cm^{-2}	650 h	[29]

4. Construction of LiF-rich solid–electrolyte interphases

4.1. Construction of LiF/compound interphases

The inherent chemical and mechanical instability of native SEI layers results in a low CE of the dendritic Li stripping and plating processes. This limitation not only limits battery lifespan but also causes short-circuit hazards. Enhancing the Young's modulus (*E*) can effectively prevent Li growth. Therefore, considerable effort has been invested in developing F-rich artificial SEI layers with higher shear modulus, primarily incorporating compounds like LiF. Re-

searchers have explored the use of oxides, fluorides [31], metal phosphates, and 2D materials to construct SEI layers with high shear moduli. By optimizing the SEI's surface energy (γ), the transportation of Li atoms through the interfacial phase can be enhanced. Furthermore, a high E can hinder the penetration of Li dendrites into the SEI. The γE criterion is a valuable tool for evaluating the ability of materials to suppress Li dendrite formation. DFT screening has revealed that SrF_2 possesses a higher γE value compared to LiF, despite LiF having the greatest γE value among all Li compounds found in native SEIs (Fig. 5(a)) [43]. Therefore, Liu *et al*. [44] immersed a Li–Sr alloy anode containing 11wt% Sr, into a LiFSI–DME (2.0 M) electrolyte. Both Li and Sr possess lower reduction potential (Li at −3.04 V and Sr at −2.89 V) than the electrolyte, enabling them to simultaneously release electrons and interact with dissociated F^- to fabricate a LiF/SrF_2-rich SEI with strong dendrite suppression ability. It has also been reported that electrically insulating NaF, similar to LiF, can inhibit vertical dendrite formation [32,44]. NaF boasts a higher E and γ compared to LiF (Fig. 5(a)), facilitating Li^+ migration in the carbon anode (γE_{NaF} = 3.16 eV·Å^{-2}·GPa, γE_{LiF} = 3.05 eV·Å^{-2}·GPa) [45]. The robust SEI of fluorinated etching (FE)–Li/Na, formed by sequential soaking in $NaPF_6$ and $LiPF_6$ electrolytes, effectively enhanced the prevention of dendrite formation during prolonged cycling. This approach contrasts with the use of $LiPF_6$ in an EC/DEC electrolyte, where the native film undergoes an acid-base reaction to form FE–Li layer. While this weak SEI helped prevent harmful reactions between the electrolyte and LMA, it lacks the durability needed to resist rupture caused by long-term cycling. The effective hybridization of LiF with SrF_2 and NaF resulted in SEIs featuring polycrystalline inorganic nano-LiF, NaF, and organic/polymer matrix structures (Fig. 5(b)). The significant deformation observed in the Li lattice near the NaF/Li and SrF_2/Li interphases suggests more robust interfacial interactions between NaF (or SrF_2) and Li compared to those with LiF/Li (Fig. 5(c)). The LiF/SrF_2- and LiF/NaF-rich SEIs exhibited reduced crystallinity and a significant presence of grain boundaries endowed with a high E and y for Li, which synergistically promoted the rapid lateral transport of Li^+ across the interphase, making Li nucleation more homogeneous and faster.

Similarly, the functionalization of 2D materials with LiF offers a promising strategy to tailor their physicochemical properties. By selectively depositing chemically and electrochemically stable LiF using online ALD at the point defect sites of hexagonal boron nitride (h-BN), it is possible to create molecular sutures that seal polycrystalline chemical vapor deposition h-BN [46]. These mechanically and chemically stable LiF/h-BN hybrid films effectively inhibited Li dendrite growth during the initial Li deposition and subsequent cycling on Cu foils. This enhancement is evidenced by the improved cycling performance of Li electrodes, achieving over 300 cycles with high CEs exceeding 95%. The widespread application of LiF in inhibiting interfacial dendrite growth extends its advantages to resist the strong sensitivity of Li metal in humid atmospheres. An ideal hy-

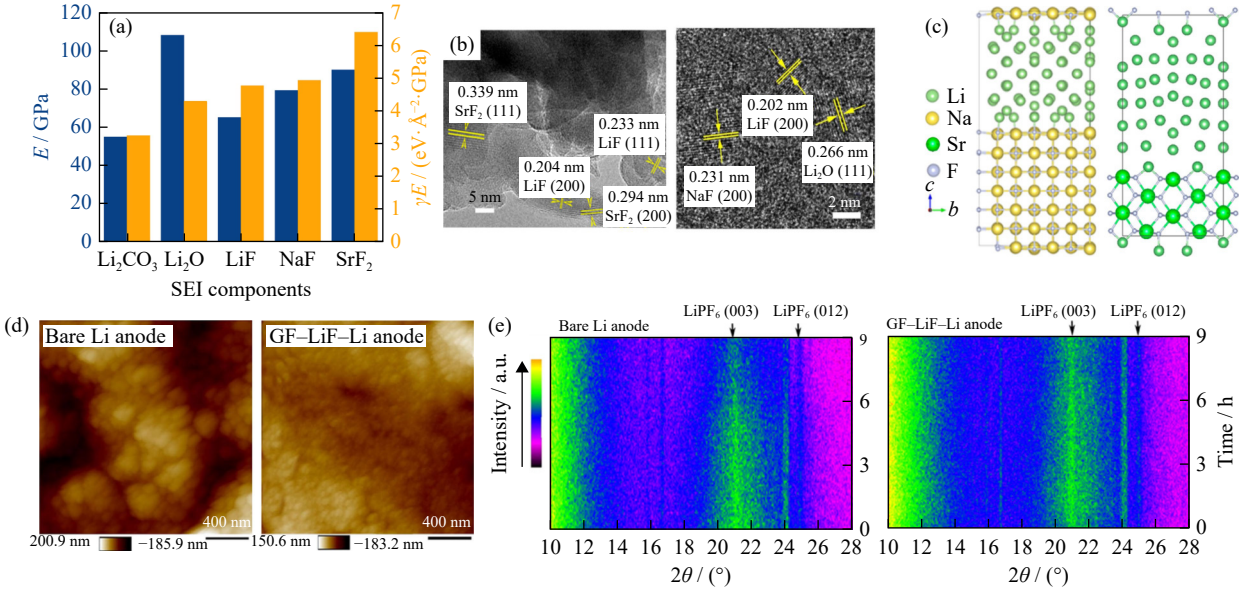

Fig. 5. (a) Comparison of E, interfacial energy γ, and Li dendrite suppression ability γE for different interphase components. (b) Acquired high-resolution (HR) TEM images for the SEI of the Li–Sr and FE–Li/Na anodes. (c) Atomic structures of (left) NaF/Li and (right) SrF_2/Li interfaces calculated by DFT. (d) Atomic force microscopy topography images of SEI on bare Li foil after the charging–discharging cycle and GF–LiF–Li at room temperature [47]. (e) Color plots represented *in situ* XRD patterns of bare Li anodes (top) and GF–LiF–Li anodes (bottom) upon the first charge–discharge process [47]. (b) Reprinted with permission from S.F. Liu, X. Ji, J. Yue, *et al*., *J. Am. Chem. Soc.*, 142, 2438-2447 (2020) [44]. Copyright 2020 American Chemical Society. (c) Reprinted with permission from Y.L. Wang, F.M. Liu, G.L. Fan, *et al*., *J. Am. Chem. Soc.*, 143, 2829-2837 (2021) [43]. Copyright 2021 American Chemical Society, and Reprinted with permission from S.F. Liu, X. Ji, J. Yue, *et al*., *J. Am. Chem. Soc.*, 142, 2438-2447 (2020) [44]. Copyright 2020 American Chemical Society.

drophobic SEI can passivate the Li surface, eliminating the need for expensive dry chambers with relative humidity below 1% during the Li extrusion and cell assembly using LMAs in industrial production. This approach is practically useful for enabling the low-cost and safe fabrication of LMAs in standard drying chambers. Shen *et al*. [47] added fluorinated graphite (GF) powder to molten Li, creating a GF–LiF–Li anode. This process forms a LiF layer at the solid–liquid interface, resulting in a hydrophobic layer of GF–LiF. Effectiveness of the GF–LiF–Li anode in preventing Li dendrite formation was confirmed using atomic force microscopy analysis (Fig. 5(d)), which examined the surface topology of both the GF–LiF–Li and bare Li electrodes during lithium deposition. The interaction between the cantilever probe tip and the sample surface revealed the morphology of the sample. It was clearly seen that the GF–LiF–Li anode, with its relatively smooth surface and uniform coating, effectively inhibited dendrite growth. By contrast, the bare Li anode's surface appeared rough and inhomogeneous. *In situ* XRD analysis further confirmed the stability of the GF–LiF–Li anode (Fig. 5(e)), with no significant changes in the diffraction peaks observed during the charging and discharging cycles. By contrast, the bare Li anode was unable to prevent reactions with the electrolyte, leading to a gradual weakening of diffraction peaks on its $LiPF_6$ (003) and (012) surfaces. Symmetric cells based on the GF–LiF–Li cells exhibited a more consistent voltage profile and lower voltage hysteresis compared to cells with bare Li at a high current density value of 10 $mA \cdot cm^{-2}$. This demonstrates the improved cycling stability of the electrode with the protective GF–LiF layer. Related reports highlight the beneficial effects of LiF/compound hybrid modifications of the interphase on the mechanical strength, as detailed in Table 2.

Low Li^+ conductivity of the SEI results from deteriorating Li^+ diffusion kinetics across the SEI that are hindered by the relatively large ion tunneling migration potential barrier of LiF. Therefore, it is critical to increase Li^+ conductivity without compromising the rigidity of LiF-rich SEIs [10,46,50]. Yang *et al*. [49] proposed that the ion conductivity of artificial SEIs might be efficiently increased by introducing small-molecule compounds containing Li. For example, Li_3N- or Li_2S-rich Li interphases, created through chemical passivation reactions, not only offer high Li^+ diffusion rates but also resist dendrite formation [32,51]. LMAs protected by a composite layer of small-molecule compounds, consisting of LiF and sulfide (LiF/sulfide-enriched Li anode), were produced by treating Li foils with 2-(fluorosulphonyl)difluoroacetic acid (Fig. 6(a)) [49]. Finite element simulations of the SEI during Li deposition, coupled with the "System III Current Distribution, Nernst-Planck" physics module (Fig. 6(b) and (c)), revealed a tendency for Li^+ to accumulate around the nuclei on the pristine Li surface. Moreover, the current density near these heterogeneous nuclei was found to be higher compared to other areas. Conversely, the LiF/sulfide-enriched Li anode demonstrated uniform Li deposition devoid of dendrites owing to its protective coating that optimizes ion distribution at the interface. The interfacial Li conduction is enhanced by the protective coating's ability to reduce side reactions. A systematic comparison of the improvement in interfacial Li^+ conduction by three Li-containing small-molecule compounds (LiF, Li_3N, and Li_2S) revealed that a co-doped LiF–Li_3N–Li_2S significantly enhanced electrochemical performance compared to SEIs enriched with only one of these compounds (Fig. 6(d)). This multiprotection strategy is achieved by the synergistic action of rationally doping Ni seeds and customizing the interfacial chemistry of the Li anode, which greatly enhances the interfacial charge–transfer kinetics. When Ni-doped Li anodes were used in conjunction with acetonitrile-based electrolytes containing lithium bis(fluorosulfonyl)imide, a uniformly constructed co-doped SEI was effectively coated with the Ni seed (Fig. 6(e)). The Ni-seeded Li anodes not only adsorb acetonitrile molecules to form a rapid Li^+-conducting SEI with the co-introduced Li_2S, Li_3N, and LiF but also serve as disperse nucleation sites, promoting the development of grainy Li deposition.

Li dendrite growth resulting from electron tunneling remains a concern despite strong mechanical strength and excellent interfacial qualities that minimize anode volume changes and encourage lateral Li deposition [52]. An uneven local electric field distribution could arise, with Li being deposited inside or outside the SEI if the SEI fails to inhibit

Table 2. Comparison of electrochemical performance parameters obtained for LiF/composite SEI on symmetric Li|Li cells

SEI components	Electrolyte	Testing condition	Cycling lifespan	*E*	Ref.
LiF/SrF_2	2 M LiFSI–DME	30 $mA \cdot cm^{-2}$, 1 $mAh \cdot cm^{-2}$	180 cycles	—	[44]
LiF/NaF	1.0 M $LiPF_6$ + EC/DEC	10 $mA \cdot cm^{-2}$	1300 h	9.56 GPa	[43]
	4 M [S] Li_2S_8 in the standard electrolyte	1 $mA \cdot cm^{-2}$, 5 $mAh \cdot cm^{-2}$	1500 h	10.5 GPa	[48]
LiF/GF	1 M $LiPF_6$/EC/DEC	1 $mA \cdot cm^{-2}$, 1 $mAh \cdot cm^{-2}$	236 h	130 MPa	[47]
		5 $mA \cdot cm^{-2}$, 1 $mAh \cdot cm^{-2}$	55 h		
		10 $mA \cdot cm^{-2}$, 1 $mAh \cdot cm^{-2}$	33 h		
LiF/h-BN	1 M $LiPF_6$ in EC/DEC	0.5 $mA \cdot cm^{-2}$, 1 $mAh \cdot cm^{-2}$	300 cycles	approaching 1.0 TPa	[46]
LiF/sulfide	1.0 M LiTFSI in DOL/DME (1:1, by volume) with 1% $LiNO_3$	1 $mA \cdot cm^{-2}$, 1 $mAh \cdot cm^{-2}$	1200 h	32.923 GPa	[49]
	1.0 M $LiPF_6$ in EC/EMC (3:7, *V*/*V*)	1 $mA \cdot cm^{-2}$, 1 $mAh \cdot cm^{-2}$	300 h		
LiF/Li_3N/Li_2S	10 M LiFSI in acetonitrile with 10vol% VC	0.5 $mA \cdot cm^{-2}$, 1 $mAh \cdot cm^{-2}$	3000 h	—	[50]

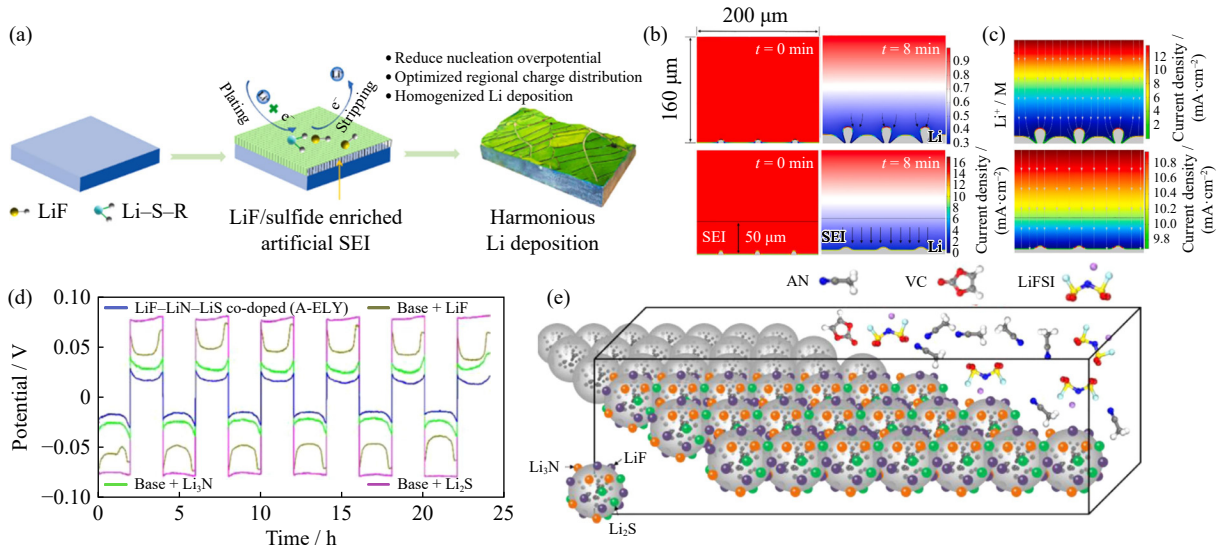

Fig. 6. (a) Schematic illustration of Li deposition on LiF/sulfide-enriched Li. (b) Li nucleation and Li^+ distribution and (c) current density distribution at the interface of (top) pristine Li and (bottom) LiF/sulfide-enriched Li. (d) Voltage profiles of symmetrical cell cycling with the Li interphases of base + LiF, base + Li_3N, base + Li_2S, or LiF–Li_3N–Li_2S co-doped interphase, attained by cycling Li foils with the control electrolytes without additive, with FEC, $LiNO_3$, and Li_2S_8 additives or A-ELY. (e) Illustration of the modified interfacial chemistry in the bulk structure of Ni-seeded Li in A-ELY. (a–c) Reprinted from *Chem. Eng. J.*, 433, J. Yang, J.M. Hou, Z.X. Fang, *et al.*, Simultaneously *in situ* fabrication of lithium fluoride and sulfide enriched artificial solid electrolyte interface facilitates high stable lithium metal anode, 133193, Copyright 2022, with permission from Elsevier. (d–e) Reprinted from *Energy Storage Mater.*, 37, Z.D. Li, L.Y. Huai, S. Li, *et al.*, Insight into bulk charge transfer of lithium metal anodes by synergism of nickel seeding and LiF–Li_3N–Li_2S co-doped interphase, 491-500, Copyright 2021, with permission from Elsevier.

electron tunneling from the LMA to the SEI [35,53]. These Li dendrites, characterized by short ion transfer channels, become "hot spots", which promote increased dendrite growth and nucleation along with heightened parasite responses [54]. Therefore, SEIs with superior electronic insulating capabilities are crucial for stable Li plating/stripping. Jin *et al.* [48] created artificial anti-electron tunneling coatings using a simple solution soaking technique, incorporating LiF and NaF nanocrystals. Compared to traditional SEIs, the LiF/NaF hybrid SEI used in Li–S batteries reduced dendritic formation, inhibited electron-blocking abilities, and enhanced ionic conductivity and mechanical strength (Table 2).

4.2. Construction of LiF/polymer composite interphases

Inorganic compounds with high shear moduli typically remain stable during Li plating/stripping, showing little morphological change. An ideal SEI withstands significant strain without fracturing, effectively blocking harmful interactions between the electrolyte and Li, thus inhibiting Li dendrite formation. Polymers and inorganic compounds have distinct characteristics. Polymers improve the flexibility and elasticity of SEI, helping it to resist significant interfacial variations [55–56]. By contrast, inorganic compounds strengthen the SEI layer. By combining these advantages, the SEI can accommodate substantial volume changes and facilitate fast Li^+ transport, protecting Li metal under high current rates. The synergistic optimization of SEI using polymers together with inorganic compounds is considered an effective approach.

The precise mechanism through which polymer functional groups and inorganic phases improve SEI stability remains unclear. Achieving a synergistic interaction between polymers and inorganic interphases on LMAs for uniform Li deposition and stable SEI layers is challenging. In addition to regulating the incorporation of organic and inorganic components in the interphase, constructing well-structured films is essential to inhibit dendrite development and extend the lifetime of LMAs. FEC is a desirable electrolyte additive for creating multifunctional protective coatings that are dense and robust, preventing undesired interactions between electrolyte and electrodes. When FEC reacts spontaneously with Li, it forms a bilayer film (Fig. 7(a)) on the LMA [57]. This reaction weakens and eventually breaks the C–F bond in FEC owing to Li–F interactions, which result from the electrical attraction between negatively charged F^- and Li^+, leading to the creation of LiF. Subsequently, organic components like CH_2CHOCO_2Li and CH_2CHOLi are produced. In the bilayer interfacial film, stiff inorganic components like LiF and Li_2CO_3 form the bottom layer, while dense organic components ($ROCO_2Li$ and ROLi) make up the top layer (Fig. 7(b)). This structure promotes uniform Li^+ deposition, prevents dendritic regrowth, and shields the LMA from corrosion caused by the organic electrolyte. In a Li|$LiNi_{0.5}Co_{0.2}Mn_{0.3}O_2$ (NCM523) cell, a mossy layer developed on the bare lithium anode after 10 cycles at 0.5 C, owing to the accumulation of dead Li and the rapid decay of pristine Li. By contrast, the LMA protected by the double-layer film showed uniform Li^+ deposition without dendrite formation, demonstrating the film stability during continuous Li plating/stripping. Polyvinylidene fluoride–hexafluoropropylene (PVDF–HFP) is extensively employed as a polymer electrolyte matrix in batteries owing to its high compatibility and chemical/elec-

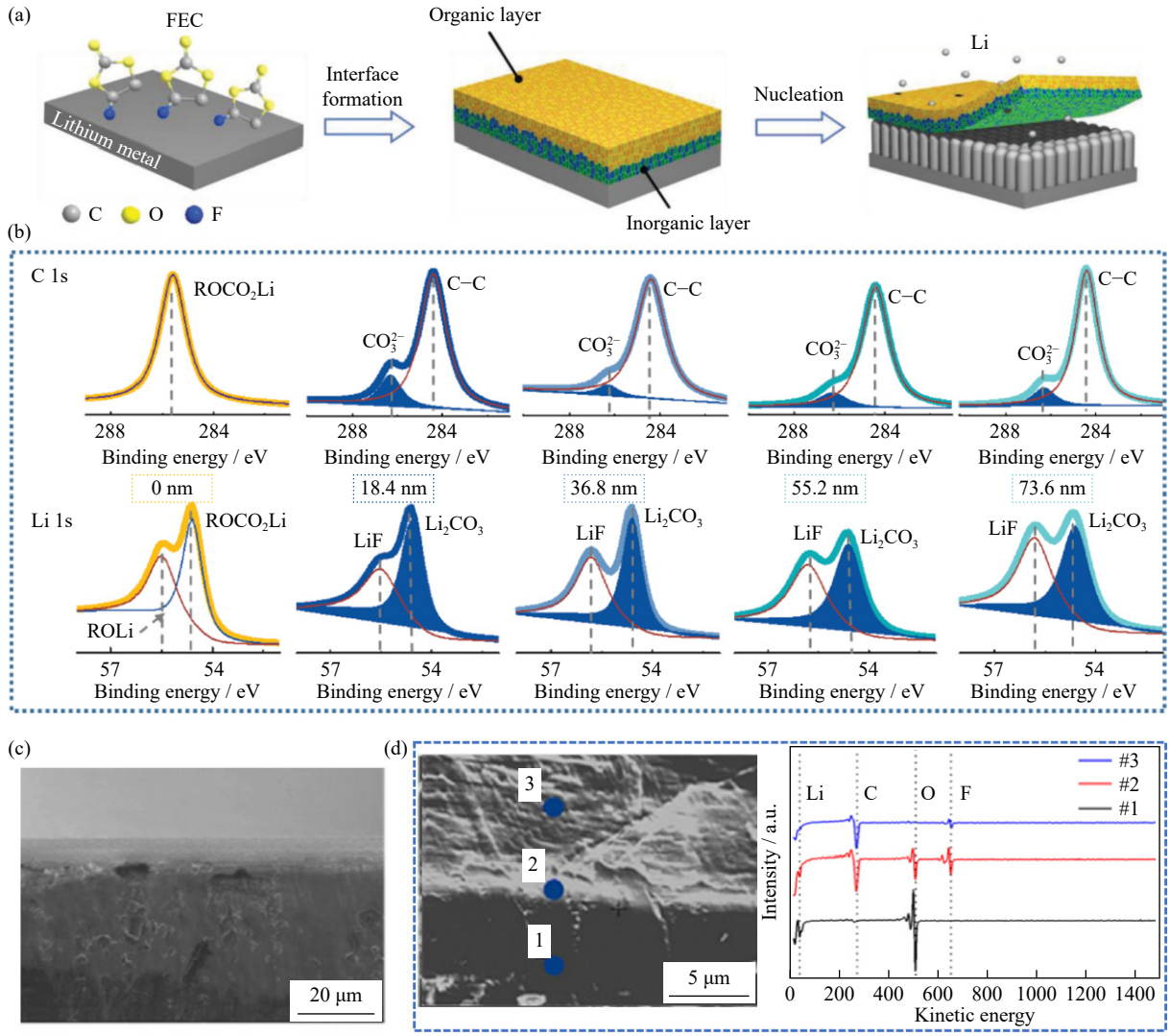

Fig. 7. (a) Diagrammatic representation illustrating the fabrication of a dual-layered film on the LMA under FEC treatments. (b) XPS peak-differentiation-imitating analysis of C 1s and Li 1s during the different sputtering layers of the protected Li. The separation distance was 18.4 nm, as calculated by the tester. (c) Obtained SEM image for CIF with a uniformly compact surface and a thickness (8 μm). (d) Elemental distribution in the cross-section of the CIF-coated Li (#1: Li side; #2: inner side of CIF (LiF-rich side); #3: outer side of CIF (PVDF-HPF-rich side) analyzed via AES. (a, b) C. Yan, X.B. Cheng, Y. Tian, *et al.*, *Adv. Mater.*, 30, 1707629 (2018) [57]. Copyright Wiley-VCH Verlag GmbH & Co. KGaA. Reproduced with permission. (c, d) Reprinted with permission from S.G. Guo, N. Piao, L. Wang, *et al.*, *ACS Appl. Energy Mater.*, 3, 7191-7199 (2020) [59]. Copyright 2020 American Chemical Society.

trochemical stability [58]. It has been proposed for use on LMA surfaces to prepare bilayer organic–inorganic composite interfacial films (CIFs) [59]. The LiF-rich internal CIF layer, located adjacent to the Li metal, promoted the formation of self-aligned columnar Li and reduced surface irregularities caused by varying current distributions. SEM image showed a uniformly dense CIF surface (Fig. 7(c)), while auger electron spectroscopy (AES) analyzed the component distribution through the depth direction of the CIF-coated Li cross-section (Fig. 7(d)). The outer CIF layer, rich in PVDF–HFP, effectively released stress and improved the flexibility of SEI. This flexible organic film effectively shielded the Li metal surface from corrosion by DEC and remained dense, uniform, and intact. The CIF-modified LMA demonstrated excellent cycling and air stabilities, as well as dendrite-free columnar deposition.

Rigid inorganic layers often struggle with maintaining good interfacial contact with LMAs, which can cause their interfacial stability to deteriorate during cycling, ultimately leading to reduced ionic conductivity. By combining an ideal soft organic or polymer component with a hard inorganic component during dynamic Li plating/stripping, a stretchable SEI layer can be developed. This hybrid SEI layer is expected to simultaneously enhance ionic conductivity while simultaneously suppressing dendrite growth in the interphase, thereby significantly reducing potential hazards and enhancing the overall electrochemical stability of LMBs. For effective design, the stretchability and adhesion of the selected organic/polymer components are two key design criteria, particularly after liquid electrolyte infiltration. Stretchability allows the SEI to accommodate changes, while adhesion is crucial for excellent interfacial contact.

The PHALF–Li negative electrode (Fig. 8(a)), developed through a photopolymerization reaction, provides moderate contact with the LMA [60]. In this process, LiF was generated *in situ* via cleaving the C–F bond in the photopolymerization of hexafluorobutyl acrylate (PHA), creating a LiF-rich artificial SEI (denoted as PHALF). This LiF-rich layer comprises inorganic LiF fillers embedded within a flexible polymer matrix, serving multiple functions: it maintains strong interaction with the LMA, adapts to volume changes, regulates Li deposition, prevents dendrite formation, and prevents adverse reactions between the electrolyte and LMA.

Poly(2,2,2-trifluoroethyl methacrylate) (PTFEMA) exhibits the typical properties of methacrylate monomers and F-containing monomers, which exhibit strong electron delocalization. This helps reduce interfacial impedance by encouraging Li polymerization, allowing the *in situ* formed protective layer to closely adhere to the concave LMA surface. A light-white, flexible 3D film was fabricated *in situ* by cross-linking PTFEMA with bifunctional $LiNO_3$, and this protective layer was applied using the blade coating method [61]. The presence of fluorine functional groups ensures that a stable, Li-rich inorganic phase fills the porous PTFEMA-N film during cycling. This phase works in harmony with the functional inorganic salt, increasing the disassociation degree of the electrolyte and improving the interfacial Li^+ conductivity (Fig. 8(b)). The hybrid organic–inorganic, rich in LiF/Li_3N, features a greater lowest unoccupied molecular orbital (LUMO) energy level and a wider LUMO–highest occupied molecular orbital (HOMO) energy gap, which theoretically confers good electrochemical performance to the LMA. The deposited Li exhibited a dense, dendrite-free structure with large, rounded particles, and distinct organic–inorganic mixed interfacial phases. After 500 cycles, the cross-section reveals a compact Li coating, unlike the pristine Li surface that showed distinct dendrites. In Li|Cu cells, the electrochemical performance was enhanced, dis-

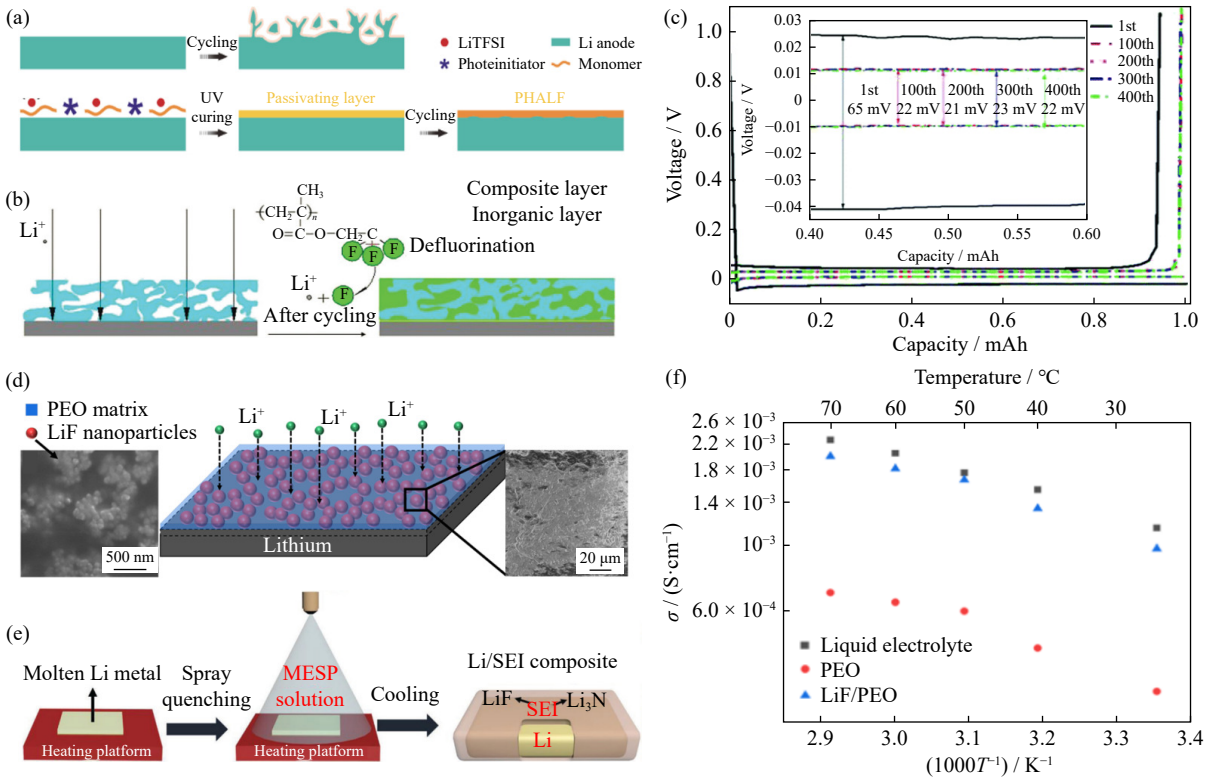

Fig. 8. (a) Diagrammatic representation for the molecular-level development of an *in situ* fluorinated SEI layer. Design of an electrolyte-based SEI through electrolyte decomposition on pure LMA (top). Production of an *in situ* fluorinated synthetic SEI through the photopolymerization process. The products produce a compact film that prevents electrolytes from reaching the surface, while LiF is produced on-site (at the bottom). (b) Graphic illustration of the PTFEMA-N layer-protected Li. (c) Acquired voltage curves for the Li|Cu cells with the PTFEMA-N layer-modified Cu foil cycled for various numbers of cycles at current density values of 1 $mA·cm^{-2}$ and 1 $mAh·cm^{-2}$. Inset: Respective polarization profiles. (d) Scheme (bottom) and top-view SEM images (right) of the LiF/PEO composite coating on Li metal and SEM image of LiF NPs (left) following ball milling in the absence of PEO. (e) Graphical demonstration for the preparation of OIFN-Li anode. (f) Arrhenius plot of the liquid electrolyte, PEO deposition, and LiF/PEO composite deposition. (a) Reprinted by permission from Springer Nature: *Nano Res.*, *In situ* fluorinated solid electrolyte interphase towards long-life lithium metal anodes, S.M. Xu, H. Duan, J.L. Shi, *et al.*, Copyright 2018. (b, c) Republished with permission of Royal Society of Chemistry, from *In situ* formed flexible three-dimensional honeycomb-like film for a LiF/Li_3N-enriched hybrid organic–inorganic interphase on the Li metal anode, C.W. Ma, G. Mu, H.J. Lv, *et al.*, 5, 2021; permission conveyed through Copyright Clearance Center, Inc. (d, f) Reprinted with permission from C.Y. Fu and C. Battaglia, *ACS Appl. Mater. Interfaces*, 12, 41620-41626 (2020) [62]. Copyright 2020 American Chemical Society. (e) S.F. Liu, X.H. Xia, S.J. Deng, *et al.*, *Adv. Mater.*, 31, e1806470 (2019) [63]. Copyright Wiley-VCH Verlag GmbH & Co. KGaA. Reproduced with permission.

playing an uniform Li coating on Cu electrodes shielded by the PTFEMA-N-layer. Although the initial cycle had a high overpotential of 65 mV owing to the formation of an organic ion-conducting layer in the first cycle, the overpotential dropped to 22 mV in subsequent cycles (Fig. 8(c)) and remained low owing to the enhanced ionic conductivity of the organic–inorganic layer.

SEIs having high shear moduli can efficiently inhibit Li dendrite formation. However, many of these materials do not conduct ions well, resulting in increased impedance and reduced energy efficiency in cells. To further enhance interfacial ionic conductivity, combining inorganic nanoparticles with a polymer matrix can be investigated. The material chosen for these synthetic SEI layers should offer enhanced ionic conductivity and shear modulus. Nanocomposite coatings on LMAs, like those consisting of LiF particles embedded in a polyethylene oxide (PEO) polymer matrix (Fig. 8(d)) [62] and an uniform and compact SEI made from an organic matrix infused with Li_3N and LiF nanocrystals (OIFN) (Fig. 8(e)) [63] have proven effective in enhancing the ionic conductivity of hybrid interphases. The combination of Li vacancies and reduced Li^+ surface diffusion barriers in LiF enhances the ionic conductivity of the LiF/PEO composite to 0.97×10^{-3} S·cm^{-1}, significantly higher than the 0.32×10^{-3} S·cm^{-1} seen in pure PEO. It also lowers the ionic activation energy to 0.20 eV, compared to 0.34 eV for Li^+ diffusion on LiF surfaces (Fig. 8(f)). FEC and $LiNO_3$ were converted *in situ* into LiF and Li_3N nanocrystals via a rapid transient spray quenching of modifed ether-based spray precursor (MESP) on molten Li. Meanwhile, DME and 1,3-dioxopentane (DOL) were converted into organolithium compounds, which bolster the stability and interactions among the inorganic grains. This innovative synergy between nano-organic and polymer mechanisms results in composite interphases exhibiting higher ionic conductivity and improved mechanical stability. They also effectively prevent the blockage of liquid electrolytes even under high current densities and during long-term cycling.

The unique structure of organic/polymer–inorganic composite artificial SEIs provides persistent stability and effectively prevents electrolyte decomposition. This characteristic significantly enhances the cyclic stability of SEIs and effectively inhibits dendrite growth. Li *et al*. [64] obtained Li_3PO_4 artificial SEI via the *in situ* reaction of polyphosphoric acid with Li. The synthetic SEI successfully prevents dendrite formation and protects LMA from corrosion by the electrolyte. Zhao *et al*. [25] demonstrated that an uniform LiF layer on LMA effectively prevented reactions with carbonate electrolytes, thereby improving anode efficiency. The LiF-rich synthetic layer was formed by applying a separator, immersed in a PVDF–DMF solution, onto a clean Li foil, which then reacted with the Li foil [27]. Owing to the mechanical and electrochemical stability of the LiF-rich artificial SEI during the Li plating/stripping cycle, the surface of the LiF-coated LMA remained smooth without noticeable dendrites, while the Li foil maintained a dense and stable structure.

Perfluoropolyether (PFPE) is known for its electron-withdrawing fluorine content, which endows it with oxidative stability, good chemical inertness, and non-reactivity with both the LMAs and electrolytes. The low surface energy of PFPE oil enables the C–F-rich moieties to completely impregnate the entire Li anode surface. Yang *et al*. [65] proposed a novel concept of a flowable fluorinated interphase by applying PFPE oil onto the surface of Li metal electrode (Fig. 9(a)). This technique optimizes the interfacial properties by creating a layered network on the Li surface instead of the dendritic development found on the rough unmodified Li surface. The tightly stacked Li structures with nanopores promoted ionic interactions between electrolyte and Li (Fig. 9(b)), benefiting LMBs. This liquid interfacial modifier effectively manages hotspots on the Li surface and inhibits dendrite formation, thereby reducing nucleation overpotential and overall voltage polarization. The PFPE-modified interface significantly extended the battery lifespan to over 1000 h without a noticeable increase in polarization at a current density value of 0.5 mA·cm^{-2} (1.5 mAh·cm^{-2}) (Fig. 9(c)).

Polymer matrix artificial protective layers (APLs) with embedded LiF particles in a PVDF–HFP hybrid effectively prevent random Li deposition and isolated Li formation, ensuring a smooth, dendrite-free topology on LMAs. These layers also help conserve both the electrolyte and Li metal [58]. However, under a deposition current density of 0.5 mA·cm^{-2} (1.0 mAh·cm^{-2}), the boundary between Li and PVDF–HFP shows significant fluctuations because the rigidity of PVDF–HFP alone is insufficient to distribute the Li coating (Fig. 9(d)). Owing to the incorporation of LiF particles having a shear modulus of 55 GPa, the APL demonstrated an E of 6.72 GPa, much higher compared to the pristine SEI at 150 MPa. This combination provides an uniform morphology and highly flexible shape. The synergy between the soft PVDF–HFP matrix, and the robust LiF particles extends the battery's cycling lifespan, prevents dendrite penetration, and enhances cycle stability. Optimizing the stabilized interface further increased the longevity of APL-modified Li|Cu full batteries to 120 cycles, maintaining an average CE of 97.2% at 0.5 mA·cm^{-2} (Fig. 9(e)).

Gao *et al*. [66] further improved the interphase performance and optimized electrolyte usage in battery production to maintain a stable interface and restrain electrolyte loss, even under lean electrolyte conditions. They created a novel reactive polymer composite (RPC) consisting of poly(vinylsulfonylfluoride-2-vinyl-1,3-dioxolane) combined with a graphene oxide 2D sheet. This composite was crafted to stabilize Li negative electrodes effectively, serving as a precursor for fabricating a stable polymer–inorganic SEI on LMAs. Cryo-TEM images demonstrate that the RPC-based SEI has a three-layer nanostructure: Li layer, RPC-based SEI layer, and a layer of unreacted RPC (Fig. 9(f)). In tests using NCM523 as the cathode material, LMBs with the RPC-based SEI operated with limited amount of electrolyte (12 μL·mAh^{-1}) and a large amount of Li (400 μm Li foil). These batteries exhibited capacity retention of 77.1% after 600 cycles (Fig. 9(g)).

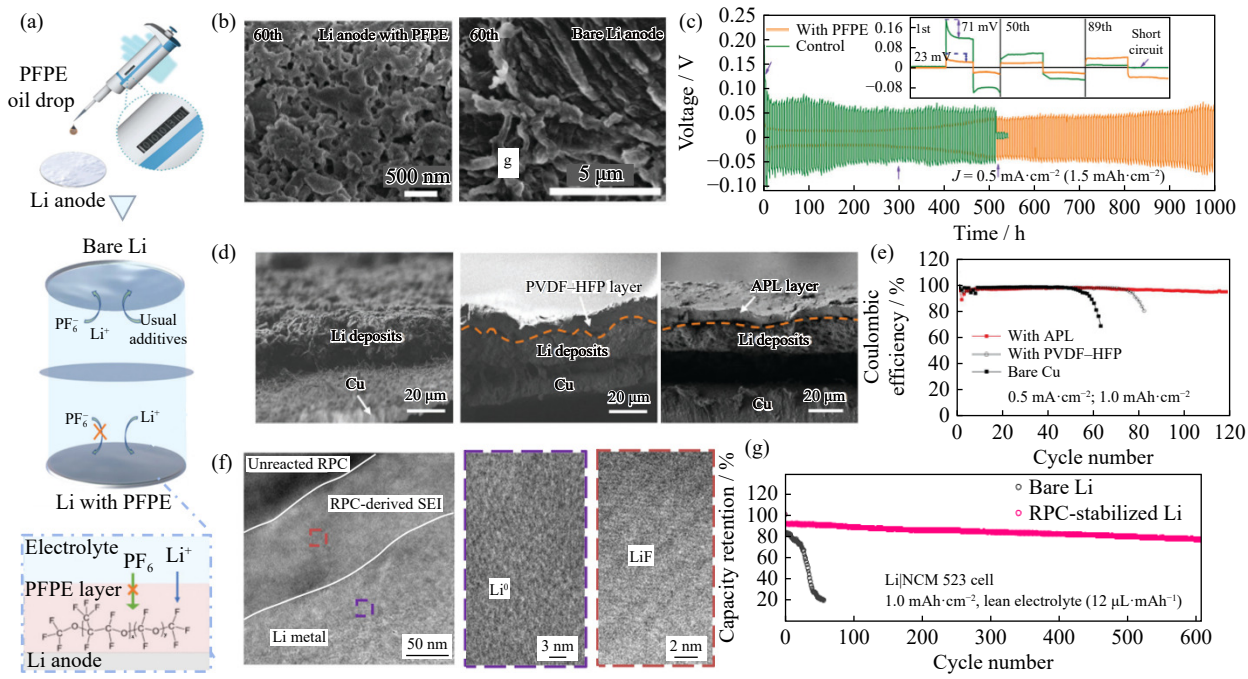

Fig. 9. (a) Diagram depicting the oil-drop technique employed on the electrode surface. (b) Acquired SEM images for the surface of the Li anode without and with PFPE modification in the plating state following 60 complete cycles. (c) Electrochemical performance and respective polarization evolution of Li/Li symmetric cells without and with PFPE modification in $LiPF_6$–EC–DMC systems at a current density value of 0.5 $mA·cm^{-2}$ (1.5 $mAh·cm^{-2}$). Insets: comparing the magnified Li plating and stripping curves at various cycling periods. (d) Cross-sectional SEM images for coated Li (1.0 $mAh·cm^{-2}$) on bare Cu (left), PVDF–HFP-modified Cu (middle), and APL-modified Cu (right) foils at a current density (0.50 $mA·cm^{-2}$). (e) CE of Li|Cu half cells (current density: 0.5 $mA·cm^{-2}$; capacity: 1.0 $mAh·cm^{-2}$). (f) Cryo-TEM images of the interphase of RPC-based Li (left); squared region of the captured HR-TEM image of the Li layer (middle); squared region of the captured HR-TEM image of the RPC-based SEI layer (left). (g) Cycling stability of Li|NCM 523 cells performed at 12 $μL·mAh^{-1}$ electrolyte and 120 μm Li foil. (a–c) Republished with permission of Royal Society of Chemistry, from C–F-rich oil drop as a non-expendable fluid interface modifier with low surface energy to stabilize a Li metal anode, Q.F. Yang, J.L. Hu, J.W. Meng, and C.L. Li, 14, 2021; permission conveyed through Copyright Clearance Center, Inc. (d, e) R. Xu, X.Q. Zhang, X.B. Cheng, *et al.*, *Adv. Funct. Mater.*, 28, 1705838 (2018) [58]. Copyright Wiley-VCH Verlag GmbH & Co. KGaA. Reproduced with permission. (f, g) Reprinted by permission from Springer Nature: *Nat. Mater.*, Polymer–inorganic solid–electrolyte interphase for stable lithium metal batteries under lean electrolyte condition, Y. Gao, Z.F. Yan, J.L. Gray, *et al.*, Copyright 2019.

The study also compares the mechanical strength and ionic transfer benefits of LiF/polymer hybrid modifications to the interphase, as shown in Table 3.

4.3. Construction of LiF/metal composite interphases

Artificial interphases with mixed conductivity interface (MCI) properties have garnered significant attention for their dual functionality in facilitating the transfer of both electrons and Li^+. These interphases incorporate various lithiophilic particles, creating a mixed electronic/ionic conductor interphase composite on the Li surface via the reaction of metal fluorides or other lithiophilic metals with Li metal. The ideal SEIs exhibit high electronic insulation and Li^+ ionic conductivity. MCIs serve as a transmission channel for SEIs, applicable not only in non-aqueous electrolytes but also in SSEs [67]. Most SSEs can interact with LMAs to form interfacial layers, which may be either SEIs or MCIs. However, MCI films often face instability and undergo electron transfer to SSEs, requiring the application of a stabilized SEI layer for effective LMB operation [68]. Despite this, MCI films can serve as an inner layer within SEI films, improving both ionic conductivity and electrochemical stability. MCIs support LMAs by facilitating preferential Li storage, offering high ionic conductivity and high *E*. Typically, the rough surface of bare Li causes an inhomogeneous electric field, where Li^+ ions accumulate at protrusions, forming dendrites that can cause internal short circuits. The interphase combines the advantages of both electron conductor and ion conductor coatings. This dual functionality facilitates efficient electron transfer and guides Li^+ during plating/stripping. Operating in a state that balances insertion capacity and supercapacitor storage, this interphase ensures fast Li^+ transfer and storage [69]. It plays a crucial role in regulating Li^+ diffusion, promoting homogenous Li coating and reducing reaction polarization. These enhancements lead to longer battery life cycles and minimize adverse reactions between the electrode and electrolyte. Numerous studies highlight the fundamental and practical applications of MCIs in energy storage, demonstrating their ability to conduct electrons while maintaining high battery performance [51,70–71].

Currently, MCI-protected LMAs can be easily created by quickly treating Li metal with a precursor solution. With the addition of LiF, symmetrical Li|Li cells and LMBs (with NCM cathode) with low polarization voltage, high CE, and

Table 3. Comparison of the electrochemical performance parameters obtained for LiF/polymer SEI on symmetric Li|Li cells

SEI components	Electrolyte	Testing condition	Cycling lifespan / h	*E* / GPa	Ionic transference number	Ref.
PVDF–DMF	1.0 M $LiPF_6$ in EC:DMC (1:1)	3 mA·cm^{-2}, 3 mAh·cm^{-2}	200	—	—	[27]
LiF and Li_2CO_3/CH_2CHOCO_2Li and CH_2CHOLi	1 M $LiPF_6$ in EC/DEC (1:1, by volume)	5 mA·cm^{-2}, 0.5 mAh·cm^{-2}	25	0.3–1.0		[57]
		2.5 mA·cm^{-2}, 0.5 mAh·cm^{-2}	90			
		1.0 mA·cm^{-2}, 0.5 mAh·cm^{-2}	110			
LiF-rich/ (PVDF–HFP)-rich	1 M $LiPF_6$/EC + EMC (3:7, by weight)	1 mA·cm^{-2}, 1 mAh·cm^{-2}	200	—		[59]
		0.5 mA·cm^{-2}, 3 mAh·cm^{-2}	500			
LiF/LiTFSI	1 M $LiPF_6$ in EC/DEC/DMC (1:1:1, by volume)	1 mA·cm^{-2}, 1 mAh·cm^{-2}	500	7.3		[60]
		2 mA·cm^{-2}, 2 mAh·cm^{-2}	200			
LiF and Li_3N/PTFEMA	1 M LiTFSI in DOL/DME	1 mA·cm^{-2}, 1 mAh·cm^{-2}	1000	—		[61]
		2 mA·cm^{-2}, 2 mAh·cm^{-2}	1000			
		5 mA·cm^{-2}, 5 mAh·cm^{-2}	500			
LiF/PEO	1.0 M $LiPF_6$ in EC:DMC (1:1)	1 mA·cm^{-2}, 1 mAh·cm^{-2}	1000	—	0.77	[62]
LiF/C–F	1 M $LiPF_6$ in EC/DMC (1:1, by volume)	0.5 mA·cm^{-2}, 1.5 mAh·cm^{-2}	1000	—	0.37	[65]
		1 mA·cm^{-2}, 3 mAh·cm^{-2}	550			
LiF/PVDF–HFP	1.0 M LiTFSI–DOL/DME with 2wt% $LiNO_3$	2 mA·cm^{-2}, 1 mAh·cm^{-2}	200	6.72	—	[58]

long lifespan can be obtained. For example, CuF_2 has been employed as fluorination precursor to form protective LiF/Cu-based MCI on the Li surface using a simple substitution reaction (Fig. 10(a)) [72]. Unlike typical SEl films, Cu in the replacement reaction disrupts the well-organized structure of the polycrystals, breaking them into smaller domains and enhancing Li deposition. This was attributed to Li storage in the LiF/Cu grain boundary regions of the MCI prior to deposition. The migration rate of ions (2.20×10^{-4} S·cm^{-1}) and electrons (0.81×10^{-2} S·cm^{-1}) was faster after lithiation. The monolithic and ordered structure of the MCI membranes, which includes inorganic phases and elastic organic groups, provides excellent chemical stability [73–74]. In symmetric Li|Li cells, these protected MCI membranes demonstrate superior electrochemical performance compared to traditional SEIs, especially at a high current density value of 2.5 mA·cm^{-2} (0.5 mAh·cm^{-2}) (Fig. 10(b)). After 500 cycles, the smooth surface of the protected MCI remains intact, showcasing its excellent protective capabilities. By contrast, the typical SEI develops a highly resistant, porous, and thick Li layer that significantly degrades cycling performance, ultimately leading to failure after 200 cycles (Fig. 10(g)).

Zn-nanoparticle-doped fluorinated interfacial layers offer excellent chemical stability and ion diffusion advantages [75]. Li *et al*. [75] conformally constructed a bilayer artificial SEI (called the ZnNF layer) using a spray quenching technique (Fig. 10(c)). This process utilizes 2,2,3,3-tetrafluoro-1-propanol (TFP), which reacts with Li to form LiF owing to its lower LUMO energy compared to DME. At higher temperatures, Li reacts with $Zn(NO_3)_2$ instead of $LiNO_3$ to produce a higher number of crystal nuclei and refine the grains by generating additional Zn nanoparticles. This ZnNF layer is rich in LiF and incorporates Zn nanoparticles, leading to finer grain sizes and more grain boundaries. These nanoparticles promote uniform Li^+ diffusion and function as lithiophilic locations to control the Li^+ flux (Fig. 10(h)). In the cross-section, a distinct lamellar structure is discernible, with the electrically insulating ZnNF layer situated just below the cyclic Li layer about 15 μm thick, made of densely spaced Li particles. The generation of dead Li was exacerbated when the uncoated Li electrode broke down into a powder. This results in a thick cycled Li layer (approximately 36-μm thick) that is likely to degrade cell performance.

With a higher standard reduction potential of 0.67 V compared to Li^+/Li, Mg^{2+} undergoes chemical reduction by interacting with Li, leading to the formation of Mg metal. A new strategy involves constructing a LiF-rich dual-layered SEI by applying MgF_2 thin films onto pristine copper foil using magnetron sputtering [76]. The lithophilic MgF_2 film facilitates the creation of a LiF-rich dual-layered SEl coating via irreversible reactions during stripping and plating. These reactions also produce Mg metal particles, which help lower the overpotential for Li nucleation on the collector as well as control Li plating and stripping (Fig. 10(d)). As a result, LFP|Li@MgF_2-coated Cu cells exhibited a higher average CE compared to those with standard LFPLi@Cu cells. The morphology of the Li deposited at a fixed plating capacity of 2 mAh·cm^{-2} and a current density of 1 mA·cm^{-2} proved that LiF-rich SEI enhances the uniform flow of Li^+ and facilitates the development of a dense Li plating structure (Fig. 10(i)). A PVDF binder was used to coat MgF_2 microparticles onto commercial PE separator. This process results in the *in situ* formation of an artificial SEI composed of LiF and lithophilic Mg atoms on the Li metal anode's surface through the spontaneous reaction of the MgF_2 coating when it contacts LMA (Fig. 10(e)). The PVDF polymer enhances SEI flexibility, allowing it to better accommodate volume changes during Li stripping/plating. The MgF_2 coating imparts thermal stability, excellent wettability, and enhanced mechanical modulus to the PE separator. Its low solubility in carbonate-

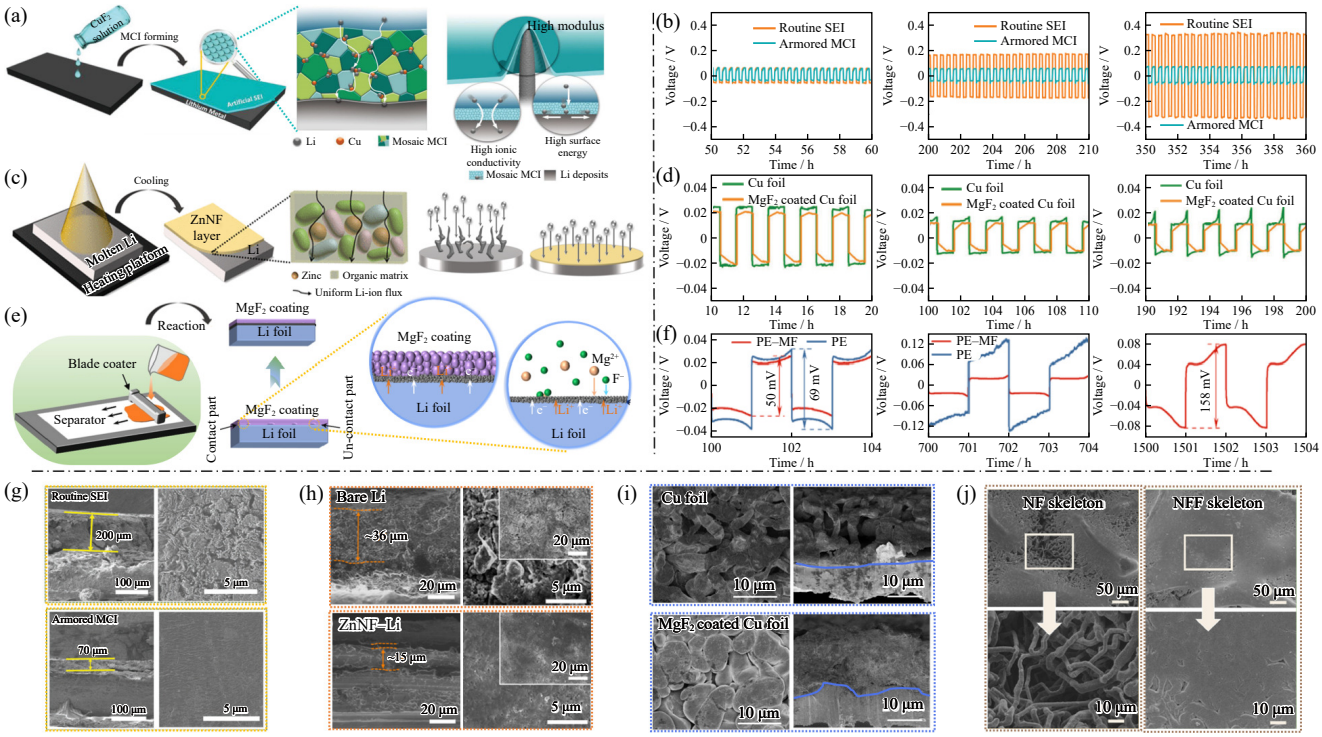

Fig. 10. (a) Graphical demonstration for the formation of the protected MCI and its impact on Li plating. (b) Voltage curves in enlarged views at 50–60, 200–210, and 350–360 h for the entire profiles for 830-h cycling at a large current density value of 2.5 mA·cm^{-2}. The typical Li|Li cells display an unstable state and experience failure following 360-h cycling. (c) Diagrammatic representation of the ZnNF layer fabrication and the effect of Li coating on bare Li and ZnNF–Li. (d) Obtained voltage–time curves in enlarged views of 10–20, 100–110, and 190–200 h are contrasted with a cycling capacity of 0.5 mAh·cm^{-2} at a current density of 0.5 mA·cm^{-2} in Li|Li@MgF_2 thin film (3 min sputtering) coated Cu foil and Li|Li@pristine Cu during Li plating/Li stripping [76]. (e) Diagrammatic representation of preparing the PE–MF separator and the fabrication of a LiF-rich synthetic SEI layer on the LMA. (f) Detailed voltage curves of Li|Li symmetric cells with PE and PE–MF separators at 1 mA·cm^{-2} with 1 mAh·cm^{-2}. (g) Cycled cross-sectional and top-view SEM images obtained for routine SEI-protected Li metal and protected MCI anodes. (h) SEM studies of bare Li and ZnNF–Li electrodes following 50 cycles (3 mA·cm^{-2}). (i) Top and side views of SEM images for the topologies of 2.0 mAh·cm^{-2} lithium plating on the pure Cu foil and MgF_2 thin film (3-min sputtering) deposited Cu foil [76]. (j) SEM analyses of the nucleation and growth behavior of Li on the NF and NFF structures during deposition with 8 mAh·cm^{-2} of Li at a current density of 1 mA·cm^{-2}. (a, b, g) C. Yan, X.B. Cheng, Y.X. Yao, *et al*., *Adv. Mater.*, 30, 1804461 (2018) [72]. Copyright Wiley-VCH Verlag GmbH & Co. KGaA. Reproduced with permission. (c, h) Reprinted with permission from J.R. Li, H. Su, M. Li, *et al*., *ACS Appl. Mater. Interfaces*, 13, 17690-17698 (2021) [75]. Copyright 2021 American Chemical Society. (e, f) Reprinted from *Chem. Eng. J.*, 442, L.W. Tan, C.L. Wei, Y.C. Zhang, Y.L. An, S.L. Xiong, and J.K. Feng, LiF-rich and self-repairing interface induced by MgF_2 engineered separator enables dendrite-free lithium metal batteries, 136243, Copyright 2022, with permission from Elsevier. (j) Reprinted from *Electrochim. Acta*, 402, W.W. Hou, S.B. Li, J.X. Liang, B. Yuan, and R.Z. Hu, Lithiophilic NiF_2 coating inducing LiF-rich solid electrolyte interphase by a novel NF_3 plasma treatment for highly stable Li metal anode, 139561, Copyright 2022, with permission from Elsevier.

and ether-based solvents ensures the consistency of the synthetic SEl produced on the LMA, which can repair occasional SEI microcracks during cycling [77]. Thus, a symmetric Li|Li cell connected using a double-sided MgF_2-coated PE separator (PE–MF) in an ether-based electrolyte exhibited stable cycling over 800 cycles for over 1600 h at a current density of 1 mA·cm^{-2}) (Fig. 10(f)). Moreover, this symmetric cell with the PE–MF separator exhibited improved multiplicative performance and a reduced overpotential compared to a symmetric cell with a PE separator when the current density increased to 0.24 mA·cm^{-2}.

Hou *et al*. [78] obtained fluorinated Ni foam (NFF) by uniformly coating a NiF_2 layer onto a Ni foam structure in an NF_3/He atmosphere. An uniform LiF-rich SEI coating formed on the NFF structure following lithiation through the rection $NiF_2 + 2Li \rightarrow 2LiF + Ni$. This coating helps alleviate undesired reactions between the electrolyte and Li while also protecting the interphase from Li dendrite formation. When the Li deposition capacity increased (ranging from 2 to 8 mAh·cm^{-2}) at a fixed current density value of 1 mA·cm^{-2}, spherical Li uniformly covered the NFF surface without generating dendrites (Fig. 10(j)) [78]. Peng *et al*. [51] fabricated a transplantable LiF-rich layer (TLL) by electrochemically reducing a NiF_2 electrode to suppress undesired reactions between Li and the electrolyte. When combined with potential measurements of Li plating on layers comprising Super-P and pure LiF powders, it was shown that Li^+ ions tend to favor deposition on Cu substrates, bypassing C and Ni particles within the TLL, promoting fresh Li deposition and inhibiting dendrite growth. The inclusion of Ni facilitates the crosslink-

ing of the matrix with nano-LiF domains, significantly hindering solvent penetration. This helps TLL significantly stabilize the Li metal/electrolyte interface and impedes dendrite development. Overall, the excellent electrochemical cycling performance of the MCI stems from its compact and significantly embedded structure, providing effective and sustainable LMAs. Currently, most methods for preparing MCI-protected LMAs involve precursor solution treatments, making it feasible to scale up production for secure and durable Li metal energy storage devices. Table 4 compares various studies on how LiF/metal hybrid modifications of the interphase affect the electrochemical properties during cycling.

Table 4. Comparison of the electrochemical performance parameters obtained for LiF/metal SEI on symmetric Li|Li cells

SEI components	Electrolyte	Testing condition	Cycling lifespan / h	Ref.
LiF/Cu	1 M LiTFSI in DOL/DME (*V*/*V* = 1:1)	2.5 mA·cm^{-2}, 0.5 mAh·cm^{-2}	830	[72]
LiF/ Zn	1 M $LiPF_6$ in EC/DEC (1:1 in volume) with 10wt% FEC	3 mA·cm^{-2}, 1 mAh·cm^{-2}	400	[75]
		5 mA·cm^{-2}, 1 mAh·cm^{-2}	300	
LiF/Mg	1 M LiTFSI and 2wt% $LiNO_3$ in 1:1 (by volume) DOL/DME	0.5 mA·cm^{-2}, 0.5 mAh·cm^{-2}	500	[76]
LiF/Mg	1 M LiTFSI in co-solvent of DOL/DME (1:1, *V*/*V*)	1 mA·cm^{-2}, 1 mAh·cm^{-2}	1500	[77]
LiF/Ni	1 M (LiTFSI) in DOL/DME (1:1, *V*/*V*) with 2wt% $LiNO_3$	0.5 mA·cm^{-2}, 1 mAh·cm^{-2}	1000	[78]
		1 mA·cm^{-2}, 1 mAh·cm^{-2}	1600	
		2 mA·cm^{-2}, 0.5 mAh·cm^{-2}	1000	
LiF/Ni	1 M $LiPF_6$ in 1:1:1 EC : EMC : DEC with 3% FEC	0.5 mA·cm^{-2}, 1 mAh·cm^{-2}	1000	[51]
		1 mA·cm^{-2}, 1 mAh·cm^{-2}	500	
		2 mA·cm^{-2}, 1 mAh·cm^{-2}	420	

4.4. Construction of LiF/alloy composite interphases

The alloy layer has been used to control homogeneous nucleation and Li coating owing to its strong affinity for Li and high surface energy. This helps replenish depleted Li, inhibit Li dendrite formation, and promote Li^+ transfer [79–81]. Typically, precursors containing metal ions are reduced by Li to form mixed inorganic and metal/alloy composites. However, these cells suffer from severe capacity degradation owing to the restricted electron insulation of the alloy layer, which experiences severe volume fluctuations during cycling. The electron conductivity of the passivation interphase also affects the deposition location of Li. Despite its low ionic conductivity, LiF offers high electronic insulation, ultrahigh thermodynamic stability, and low diffusion energy barrier, ensuring uniform Li coating. Therefore, several scholars are exploring the efficient integration of inert LiF and electrochemically active Li-based alloy layers to construct robust artificial SEI layers with high LMA stabilities [82].

The topology of Li metal deposition is intricately connected to the initial deposition and nucleation growth behavior on the Li electrode surface. Creating Li-based alloy layer *in situ* as a protecting coating on Li electrodes can considerably lower the barriers to Li nucleation, promoting homogeneous Li coating. The Li_3Mg_7 alloy serves as an ideal nucleation site for Li owing to its strong affinity, ensuring a uniform Li coating. LiF enhances mechanical strength, providing stability during cycling and preventing direct contact between the Li anode and the electrolyte. By combining the Li-attracting properties of the Li_3Mg_7 alloy with the robust mechanical strength of LiF, the MgF_2@Li electrode effectively lowers cyclic overpotential, improves cyclic stability, and extends the cycling lifespan [83].

Focusing solely on enhancing the mechanical characteristics and electrochemical stability may lead to significant volume changes [82]. Combining the advantages of organic/inorganic composite artificial SEIs, creating an inorganic-rich composite SEI from *in situ* generated inorganic SEIs derived from organic SEIs can prevent the direct combination of organic/inorganic SEIs. Gan *et al.* [84] proposed the *in situ* generation of dense, organic/inorganic dual-functional LiF-rich PVDF-based SEIs (DFPIs) using an InF_3-PVDF coating on Li. These DFPIs help avoid poor interfacial contact and agglomeration of inorganic SEI particles, which can occur owing to the high surface energy and inherent poor compatibility of organic SEIs, leading to the inhomogeneous distribution of mechanical strength and ionic flow [85–86]. During plating, the InF_3–PVDF coating formed the desired LiF-rich PVDF-based composite SEI and a lithophilic Li–In alloy substrate *in situ* during plating. This lipophilic substrate promoted the horizontal growth of Li, accommodating the volume changes during Li deposition, while the organic–inorganic composite layer inhibited the continuous generation of Li dendrites during cycling. This dual approach achieved good interfacial stability, fast interfacial kinetics, and significantly reduced Li dendrite growth. Lithophilic alloys can also perform well at the electrolyte–electrode interface. A MgF_2 sol-derived nano-thin layer was applied on the $Li_{6.75}La_3Zr_{1.75}Ta_{0.25}O_{12}$ (LLZTO) pellet using a glue-free spin-coating approach, resulting in an all-inorganic Li–Mg|LiF (LMF) film formed by a conversion reaction with molten Li. The LMF layer, consisting of Li–F and Li–Mg alloys with low γ, further enhances the chemical interaction between LLZTO and Li [87]. However, in Li|LLZTO|LFP cells, capacity decreases rapidly during cycling owing to poor contact at the LLZTO|Li interface and the loss of active Li from the anode.

The Sn–Li alloy phase has been shown to reduce the Li^+ diffusion potential, ensuring rapid ion diffusion and enhan-

cing the interfacial stability of Li. This alloy formation allows Li to be stored and deposited uniformly beneath it. A synthetic SEI comprising Sn, LiF, and Sn–Li alloys was obtained by reacting Li metal electrode surface exposed to an electrolyte containing SnF_2 [88]. Different artificial SEIs with different thicknesses (10, 25, and 55 μm) were prepared by treating bare Li with electrolytes containing SnF_2 at 1wt%, 3wt%, and 5wt% concentrations. Among them, the AFH-25 with a 25-μm thickness effectively protected the Li electrode, resulting in uniform, smooth, and dendrite-free Li deposition while effectively increasing its ionic conductivity to 5.84×10^{-4} S·cm^{-1}. Similarly to the use of the Li–Mg alloy to improve Li performance at the LLZTO grain boundaries, a Li_7Sn_3/LiF interfacial layer was used between the LMA and the garnet-type solid electrolyte to obtain LMBs with long cycling performance at high rates. On the surface of the garnet-type LLZTO, a mosaic Li_7Sn_3/LiF interfacial coating was produced in situ by reacting the SnF_2 coating with Li [89]. Li_7Sn_3 nanoparticles with a nanomosaic structure surrounded by LiF were constructed in this interphase (Fig. 11(a)). As evident from STEM images, both Sn and F are concentrated in region 1 near LLZT (Fig. 11(b)). Further analysis with SAED images confirmed that this area contains Li_7Sn_3 crystals. XPS sputtering results for region 1 (Fig. 11(c)) verified that Li_7Sn_3 nanoparticles and LiF coexist in region 1. The ion-insulating Li_2CO_3 on the LLZT pellet surface was eliminated by SnF_2 during the production of the interfacial layer. Thus, the interface structure decreases the ion-diffusion obstruction of LLZT to the Li anode, enabling fast Li^+ conduction.

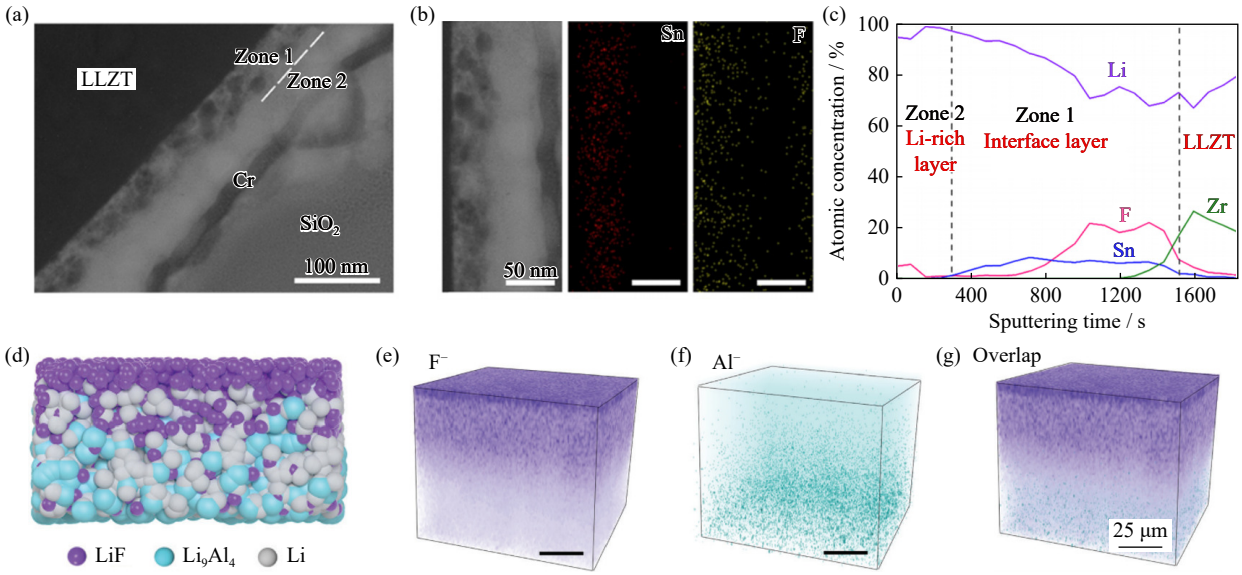

Fig. 11. (a) STEM image of the interfacial structure between LLZT and the Cr–SiO_2 protection layer. (b) STEM image of the interfacial structure and corresponding elemental distribution of Sn and F. (c) Depth profiles of atomic percentages of elements Li, Sn, F, and Zr. (d) Schematic representation of the FGLA. (e) F^-, (f) Al^-, and (g) the overlap in the ToF-SIMS sputtered volumes of the FGLA. (a–c) Reprinted with permission from B.K. Hu, W. Yu, B.Q. Xu, *et al.*, *ACS Appl. Mater. Interfaces*, 11, 34939-34947 (2019) [89]. Copyright 2019 American Chemical Society. (d–g) Republished with permission of Royal Society of Chemistry, from A self-regulated gradient interphase for dendrite-free solid-state Li batteries, T.R. Wang, J. Duan, B. Zhang, *et al.*, 15, 2023; permission conveyed through Copyright Clearance Center, Inc.

The Li/Al_4Li_9–LiF nanocomposite (LAFN) was synthesized as an optimal framework for infusing Li by investigating the "overlithiation" process of the mesoporous AlF_3 structure. In symmetric batteries, LAFN anodes can operate at an unprecedented high current density of 20 mA·cm^{-2} [90]. The Al_4Li_9–LiF nanoparticles generated therein exhibited high degree of lithophilicity, resulting in minimal volume changes during lithium stripping/plating, effectively preventing dendrite formation. This design concept was further applied to the solid-state electrolyte interface to form a functional gradient Li anode (FGLA) through a self-regulated reaction between molten Li and AlF_3 (Fig. 11(d)) [91]. Depth-profiling time-of-flight secondary-ion mass spectroscopy (ToF-SIMS) effectively revealed the 3D structure of FGLA over sputtering time. Li_9Al_4, owing to its strong lithophilicity, is positioned on the Li side, reducing interfacial resistance (Fig. 11(e)). Alternatively, with its high interfacial energy and electron-insulating properties, LiF is on the other side, effectively suppressing dendrite growth (Fig. 11(f)). This results in an effective gradient self-regulating interfacial structure (Fig. 11(g)). Inspired by this, researchers explored electroless plating of aluminum fluoride (AlF_3) on Li metal immersed in a supersaturated AlF_3 solution in a carbonate electrolyte. The reaction between the AlF_3 layer and Li produced a bifunctional composite interphase comprising LiF for interface stabilization and Li–Al alloy that facilitates uniform coating during cycling [92]. The introduction of AlF_3 effectively adjusted the Li surface activity, affecting Li distribution at the interface, promoting rapid diffusion of surface ions, and achieving excellent morphological control. CI-NEB calculations indicated that Li atoms diffuse rapidly between two neighboring hollow adsorption sites on the Al (111) sur-

face with a reduced activation energy barrier of 21 meV, while the diffusion barrier on the Li_9Al_4 (100) is 73.5 meV (Fig. 12(a)). This indicates that the surface of the composite interfacial mixture has excellent Li diffusion capabilities, promoting homogeneous Li coating and effectively preventing dendrite formation. Song *et al*. [93] proposed inserting a carbon cloth containing a 3D structure between the LMA and the separator, along with a coating layer comprising lithiophilic AlF_3 (ACC). Similarly, Wang *et al*. [94] proposed using PVDF–HFP/AlF_3-modified Celgard separators. Owing to the *in situ* reaction of AlF_3 with highly reactive Li, LiF-rich SEIs were formed, containing composite components such as LiF, Li_2O, and Li–Al. After plating, the microstructure of the AlF_3-coated carbon cloth-modified anode surfaces showed uniform Li agglomeration and plating morphology without visible carbon cloth, indicating that the lithiophilic AlF_3 on the carbon cloth was crucial for ensuring homogeneous Li plating. This indicates that the SEI layer consisting of Li–Al alloys and LiF helps to suppress the increase in impedance and enhances rate capability.

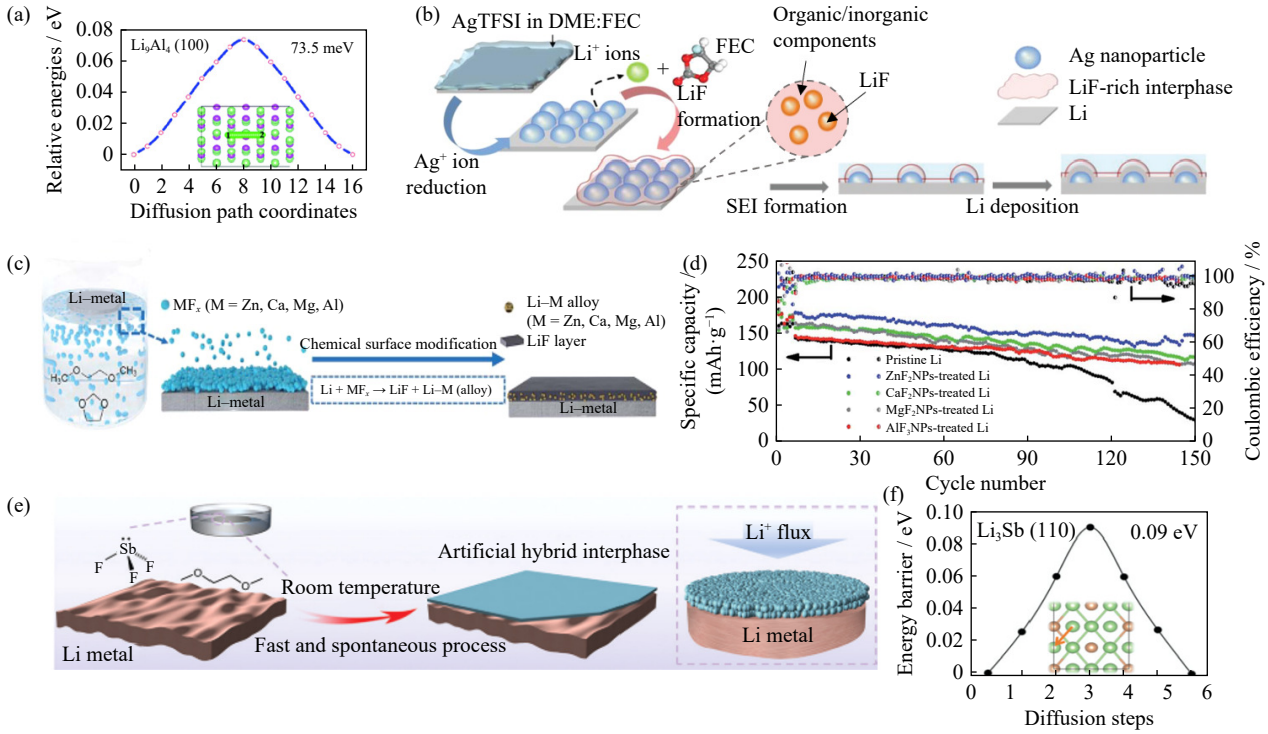

Fig. 12. (a) DFT calculated energy differences of Li^+ diffusion on Li_9Al_4 (100) surfaces. (b) Schematic diagram illustrating the fabrication of Li–Ag–LiF surface, along with the synergetic regulation of nucleation and SEI for Li plating. (c) Graphic representation of the synthetic SEI layer fabrication by promoting the reaction of highly dispersible metal fluoride nanoparticles (M = Al, Mg, Ca, and Zn) on the LMA surfaces [95]. (d) Electrochemical cycling performance at 0.5 C of cells employing the pristine Li metal anode and MF_xNP-treated LMAs in the 10th and 15th cycle, respectively [95]. (e) Graphic representation of the hybrid LiF/Li_3Sb interphase on Li foil. (f) Kinetic energy barriers of Li^+ diffusion on the Li_3Sb (110) surfaces. The arrows in orange color depict the diffusion routes on the surfaces. (a) Republished with permission of Royal Society of Chemistry, from Dendrite-free and air-stable lithium metal batteries enabled by electroless plating with aluminum fluoride, Z.S. Wang, Z.M. Xu, X.J. Jin, *et al*., 8, 2020; permission conveyed through Copyright Clearance Center, Inc. (b) Z. Peng, J.H. Song, L.Y. Huai, *et al*., *Adv. Energy Mater*., 9, 1901764 (2019) [79]. Copyright Wiley-VCH Verlag GmbH & Co. KGaA. Reproduced with permission. (e, f) Republished with permission of Royal Society of Chemistry, from An artificial hybrid interphase for an ultrahigh-rate and practical lithium metal anode, A.J. Hu, W. Chen, X.C. Du, *et al*., 14, 2021; permission conveyed through Copyright Clearance Center, Inc.

The solubility of metal fluorides in electrolytes is generally low, but using nanoparticles offers an effective approach for dispersing insoluble metal fluoride materials in solutions. Moreover, metal fluoride nanoparticles can be synthesized using simple solution methods, significantly reducing costs for large-scale industrial production. Peng *et al*. [79] treated Li metal surfaces with a solution containing an Ag^+ precursor, specifically silver bis(trifluoromethanesulfonyl)imide (AgTFSI) in DME/FEC. Owing to the high oxidation potential of Ag^+, Li^+ reduced by Ag interacted efficiently with F^- released from FEC, forming a cross-linked, LiF-rich interphase with numerous Ag nanoparticles on the Li surface (Fig. 12(b)). These Ag nanoparticles, which strongly attract Li atoms, enhanced charge–transfer kinetics on the Li surface. This enabled the Li–Ag/Li and Li–Ag–LiF/Li electrodes to achieve exchange current densities (3.12 and 3.24 $mA \cdot cm^{-2}$, respectively) at overpotential (0 mV), compared to the bare Li electrode (2.51 $mA \cdot cm^{-2}$). This improvement was evident in the deposition morphology, wherein small, granular deposits of Li were evenly spread across the Li–Ag–LiF and Li–Ag surfaces, unlike the typical dendritic structures found on bare Li. The DFT model explains this by showing that the adsorption energy of Li atoms on various Ag surfaces is typically greater compared to the binding en-

ergy on the Li surface. Therefore, Ag nanoparticles serve as efficient Li nucleation sites, significantly decreasing nucleation overpotential, improving Li plating morphology, and effectively protecting LMAs from long-term cycling.

Using salts and fluorinated additives in electrolytes can be costly. Li *et al*. [95] reported the formation of functional LiF/Li–M alloy layers without *in situ* generation (Fig. 12(c)) by promoting the reaction of highly dispersible metal fluoride nanoparticles (MF_x, M = Al, Mg, Ca, and Zn) on the LMAs surface by inserting fresh Li foils in a suspension of MF_x. Symmetric cells consisting of LMAs protected by LiF/Li–Zn alloy layers exhibited extended and consistent voltage profiles (around 220 mV during the initial 50-h cycle) and could operate for up to 100 h at polarization voltages below 400 mV. The cells with LiF/Li–M alloy layers protecting the LMA maintained a sustained discharge capacity, showing minimal capacity decay (Fig. 12(d)). The detailed charge/discharge voltage distribution indicates reduced polarization and more stable cycling of the full battery employing the protected LMA, verifying the efficiency of the synthetic SEI protective layer formed in practical LMBs. To improve ionic conductivity and offset the enhanced ion tunneling migration barrier of LiF, Li was immersed in nonprotic DME with SbF_3 (Fig. 12(e)), resulting in the inclusion of Li_3Sb into the LiF-rich SEI layer [53]. The Li_{2nd}-top site (identified as the most stable position for the adsorbed Li^+ among the four possible sites on the Li_3Sb (110) surface) on the Li_3Sb (110) surface proved to be the most stable for Li adsorption, with an adsorption energy of 1.04 eV, while the most stable Li site on the surface on the LiF (001) F-top site had an adsorption energy of 0.71 eV. The energy barriers for Li diffusion on LiF (001) and Li_3Sb (110) were 0.28 and 0.09 eV, respectively, both lower than the energy barrier observed for the Li (001) surface, which was 0.39 eV (Fig. 12(f)). This alloyed artificial hybrid interphase enhanced Li adsorption and diffusion, thanks to the combined effect of Li_3Sb as a superionic conductor stabilizing the SEI interface, and LiF, which effectively blocked electrons from tunneling from the LMA to the SEI. Liquid-phase reactions can also be combined with Li substrate modifications. A porous composite Li electrode, formed through the spontaneous reaction of molten Li with a sulfur/carbon nanofiber matrix, served as the substrate. This modified substrate was then incorporated into the BiF_3–P_2S_5 complex, which reacted spontaneously to form a Li_3Bi alloy. This process securely attached LiF to the Li surface, thus achieving a porous Li electrode shielded by functional composites. Related reports comparing the impact of LiF/alloy hybrid modifications of the interphase on electrochemical properties during cycling are compared in Table 5.

Table 5. Comparison of the electrochemical performance parameters obtained for LiF/alloy SEI on symmetric Li|Li cells

SEI components	Electrolyte	Testing condition	Cycling lifespan / h	Ref.
LiF/Li_3Mg_7	1 M LiTFSI DOL/DME (1:1, *V*/*V*)	0.5 mA·cm^{-2}, 1 mAh·cm^{-2}	1800	[83]
		1 mA·cm^{-2}, 1 mAh·cm^{-2}	1200	
LiF/Li–Mg	$Li_{6.75}La_3Zr_{1.75}Ta_{0.25}O_{12}$	0.3 mA·cm^{-2}, 0.15 mAh·cm^{-2}	1000	[87]
LiF/Li_5Sn_2	1M $LiPF_6$ in EC/DEC (1:1, *V*/*V*)	0.5 mA·cm^{-2}, 1 mAh·cm^{-2}	2500	[88]
		1 mA·cm^{-2}, 1 mAh·cm^{-2}	800	
LiF/Li_7Sn_3	$Li_{6.75}La_3Zr_{1.75}Ta_{0.25}O_{12}$	0.1 mA·cm^{-2}, 0.05 mAh·cm^{-2}	1000	[89]
		0.1 mA·cm^{-2}, 0.1 mAh·cm^{-2}	200	
LiF/Al_4Li_9	1 M $LiPF_6$ in 1:1 EC/DEC with 10% FEC and 1%VC	1 mA·cm^{-2}, 1 mAh·cm^{-2}	194	[90]
		10 mA·cm^{-2}, 1 mAh·cm^{-2}	194	
		20 mA·cm^{-2}, 1 mAh·cm^{-2}	9	
LiF/Li–Al	1 M $LiPF_6$ in EC/DEC/EMC (3:2:5, by weight)	1 mA·cm^{-2}, 1 mAh·cm^{-2}	800	[92]
		3 mA·cm^{-2}, 1 mAh·cm^{-2}	500	
		5 mA·cm^{-2}, 1 mAh·cm^{-2}	100	

5. Conclusions and prospects

The SEI plays a pivotal role in LMBs for generating and storing electricity by effectively passivating the electrode and preventing undesired reactions with the electrolyte. Establishing stable SEI is essential for ensuring the prolonged functionality of batteries. LiF has garnered attention for its ability to stabilize LMAs. Studies have shown that F-rich interphases are pivotal for promoting uniform Li transport, passivating the electrode at the electrolyte interface, and enhancing mechanical stability by decreasing Li dendrite development. Herein, we reviewed the recent research progress on optimizing the preparation of LiF passivation interphases for protecting Li metal electrodes and discussed four types of materials, namely compounds, polymers, metals, and allows that synergistically enhance SEI performance with LiF. By summarizing research progress and the effects of various hybrid fluorinated interphases, researchers can better understand the challenges in the construction of fluorinated interphases.

(1) Progress has been made in developing high-quality, continuous LiF coatings to ensure uniform Li deposition. By continuously improving fluorination methods from simple electrolyte additives to gas-phase deposition, the produced LiF layer is homogeneous, continuous, conformal, and dense, effectively inhibiting dendrite growth and preventing the

formation of dead Li to reduce the ion kinetic barriers. However, the relatively reduced Li^+ conductivity of LiF negatively affects the mass-transfer kinetics of LMAs, leading to decreased electrochemical performance of cells. Addressing these adverse effects is crucial for further enhancing the electrochemical performance and stability of fluorinated interphases.

(2) Compounds such as SrF_2, NaF, GF, and h-BN combined with LiF can further enhance the *E* of SEI and improve interfacial ionic conductivity without compromising mechanical strength, which can compensate for the negative effects of LiF to a certain extent. Promising results show that adding small-molecule compounds containing Li can decrease the ionic mobility barrier of synthetic SEIs owing to a high ionic diffusion rate and inhibited dendrite growth. Future research should focus on reducing electron tunneling probability while providing high ionic conductivity.

(3) Polymer introduction can significantly improve the flexibility of the F-rich interphase, allowing it to resist cycling changes. Studies have substantially improved the ionic conductivity of inorganic/organic composite SEIs. The bilayer structure of polymer–inorganic composite artificial SEIs provides durable stability and inhibits electrolyte decomposition, prolonging the cycle lifespan of the SEI. Most current structures are simple inorganic inner-organic outer structures. Future studies should address the poor interfacial stability owing to limited contact between the rigid inorganic layer and the LMA. In the future, SEIs consisting of organic-based hybridized inorganic components with highly stable structures should be investigated.

(4) Combining LiF with metal particles improves the chemical stability of the original MCI, resulting in an SEI with improved Li storage and high ionic conductivity. A F-rich MCI in the SEI's inner layer provides good electron and ion channels. However, enabling rapid Li^+ transfer and storage, along with unobstructed electron and ion channels at the anode, challenges the SEI's electron-insulating properties, requiring novel surface electrochemistry and interfacial engineering.

(5) Combining inert LiF with electrochemically active Li-based alloys effectively counteracts the negative effects of both components on the SEI. LiF, known for its electronic insulation and superthermal stability, compensates for the limited electron insulation of alloy layers, which can experience severe volume fluctuations during cycling. Alternatively, the alloy provides high surface energy and high lithophilicity. Despite efforts to improve Li plating/stripping at high current densities, dendrite formation and volume expansion remain significant challenges, hindering the practical use of F-rich alloys in SEIs. To address these issues, it is essential to develop stable electrolytes and SSEs in fluorinated alloy protective layers and construct more stable electrolyte/electrode interfaces.

Acknowledgements

The authors would like to thank the support from the National Natural Science Foundation of China (No. U2333210) and the Sichuan Science and Technology Program, China (No. 21SYSX0011).

Confict of Interest

The authors declare no competing financial interest.

References

[1] T. Placke, R. Kloepsch, S. Dühnen, and M. Winter, Lithium ion, lithium metal, and alternative rechargeable battery technologies: The odyssey for high energy density, *J. Solid State Electrochem.*, 21(2017), No. 7, p. 1939.

[2] L. Grande, E. Paillard, J. Hassoun, *et al*., The lithium/air battery: Still an emerging system or a practical reality?, *Adv. Mater.*, 27(2015), No. 5, p. 784.

[3] P. Albertus, S. Babinec, S. Litzelman, and A. Newman, Status and challenges in enabling the lithium metal electrode for high-energy and low-cost rechargeable batteries, *Nat. Energy*, 3(2018), p. 16.

[4] J. Heine, P. Hilbig, X. Qi, P. Niehoff, M. Winter, and P. Bieker, Fluoroethylene carbonate as electrolyte additive in tetraethylene glycol dimethyl ether based electrolytes for application in lithium ion and lithium metal batteries, *J. Electrochem. Soc.*, 162(2015), No. 6, p. A1094.

[5] K.Z. Cao, S.T. Wang, Y.N. He, J.H. Ma, Z.W. Yue, and H.Q. Liu, Constructing Al@C–Sn pellet anode without passivation layer for lithium-ion battery, *Int. J. Miner. Metall. Mater.*, 31(2024), No. 3, p. 552.

[6] T. Wei, Q. Zhang, S.J. Wang, *et al*., A gel polymer electrolyte with IL@UiO-66–NH_2 as fillers for high-performance all-solid-state lithium metal batteries, *Int. J. Miner. Metall. Mater.*, 30(2023), No. 10, p. 1897.

[7] W.D. Zhang, Q. Wu, J.X. Huang, *et al*., Colossal granular lithium deposits enabled by the grain-coarsening effect for high-efficiency lithium metal full batteries, *Adv. Mater.*, 32(2020), No. 24, art. No. 2001740.

[8] X.L. Chen, Y.D. Gong, X. Li, F. Zhan, X.H. Liu, and J.M. Ma, Perspective on low-temperature electrolytes for $LiFePO_4$-based lithium-ion batteries, *Int. J. Miner. Metall. Mater.*, 30(2023), No. 1, p. 1.

[9] X.B. Cheng, J.Q. Huang, and Q. Zhang, Review—Li metal anode in working lithium–sulfur batteries, *J. Electrochem. Soc.*, 165(2017), No. 1, p. A6058.

[10] X.B. Cheng, C. Yan, X.Q. Zhang, H. Liu, and Q. Zhang, Electronic and ionic channels in working interfaces of lithium metal anodes, *ACS Energy Lett.*, 3(2018), No. 7, p. 1564.

[11] Y.Y. Lu, Z.Y. Tu, and L.A. Archer, Stable lithium electrodeposition in liquid and nanoporous solid electrolytes, *Nat. Mater.*, 13(2014), No. 10, p. 961.

[12] K. Yan, Z.D. Lu, H.W. Lee, *et al*., Selective deposition and stable encapsulation of lithium through heterogeneous seeded growth, *Nat. Energy*, 1(2016), No. 3, art. No. 16010.

[13] E. Peled, Film forming reaction at the lithium/electrolyte interface, *J. Power Sources*, 9(1983), No. 3, p. 253.

[14] Y.F. Zhou, M. Su, X.F. Yu, *et al*., Real-time mass spectrometric characterization of the solid–electrolyte interphase of a lithium-ion battery, *Nat. Nanotechnol.*, 15(2020), No. 3, p. 224.

[15] G. Nazri and R.H. Muller, Composition of surface layers on Li electrodes in PC, $LiClO_4$ of very low water content, *J. Electrochem. Soc.*, 132(1985), No. 9, p. 2050.

[16] D. Aurbach, M.L. Daroux, P.W. Faguy, and E. Yeager, Identification of surface films formed on lithium in propylene carbonate solutions, *J. Electrochem. Soc.*, 134(1987), No. 7, art. No.

1611.
[17] M. Garreau, Cyclability of the lithium electrode, *J. Power Sources*, 20(1987), No. 1-2, p. 9.
[18] J. Thevenin, Passivating films on lithium electrodes. An approach by means of electrode impedance spectroscopy, *J. Power Sources*, 14(1985), No. 1-3, p. 45.
[19] J.G. Thevenin and R.H. Muller, Impedance of lithium electrodes in a propylene carbonate electrolyte, *J. Electrochem. Soc.*, 134(1987), No. 2, p. 273.
[20] S.S. Zhang, K. Xu, and T.R. Jow, Enhanced performance of Li-ion cell with $LiBF_4$–PC based electrolyte by addition of small amount of LiBOB, *J. Power Sources*, 156(2006), No. 2, p. 629.
[21] G.W. Zheng and T. Wei, Batteries: Just a spoonful of $LiPF_6$, *Nat. Energy*, 2(2017), No. 3, art. No. 17029.
[22] T.Z. Hou, G. Yang, N.N. Rajput, *et al*., The influence of FEC on the solvation structure and reduction reaction of $LiPF_6$/EC electrolytes and its implication for solid electrolyte interphase formation, *Nano Energy*, 64(2019), art. No. 103881.
[23] J. Ko and Y.S. Yoon, Recent progress in LiF materials for safe lithium metal anode of rechargeable batteries: Is LiF the key to commercializing Li metal batteries?, *Ceram. Int.*, 45(2019), No. 1, p. 30.
[24] T. Li, X.Q. Zhang, P. Shi, and Q. Zhang, Fluorinated solid–electrolyte interphase in high-voltage lithium metal batteries, *Joule*, 3(2019), No. 11, p. 2647.
[25] J. Zhao, L. Liao, F.F. Shi, *et al*., Surface fluorination of reactive battery anode materials for enhanced stability, *J. Am. Chem. Soc.*, 139(2017), No. 33, p. 11550.
[26] Y.Y. Liu, D.C. Lin, Y.Z. Li, *et al*., Solubility-mediated sustained release enabling nitrate additive in carbonate electrolytes for stable lithium metal anode, *Nat. Commun.*, 9(2018), No. 1, art. No. 3656.
[27] J.L. Lang, Y.Z. Long, J.L. Qu, *et al*., One-pot solution coating of high quality LiF layer to stabilize Li metal anode, *Energy Storage Mater.*, 16(2019), p. 85.
[28] W. Liu, J.X. Li, H.Y. Xu, J. Li, and X.P. Qiu, Stabilized cobalt-free lithium-rich cathode materials with an artificial lithium fluoride coating, *Int. J. Miner. Metall. Mater.*, 29(2022), No. 5, p. 917.
[29] S.S. Liu, Y.L. Ma, J.J. Wang, *et al*., Regulating Li deposition by constructing homogeneous LiF protective layer for high-performance Li metal anode, *Chem. Eng. J.*, 427(2022), art. No. 131625.
[30] Q.L. Zhang, J. Pan, P. Lu, *et al*., Synergetic effects of inorganic components in solid electrolyte interphase on high cycle efficiency of lithium ion batteries, *Nano Lett.*, 16(2016), No. 3, p. 2011.
[31] L. Fan, H.L. Zhuang, L.N. Gao, Y.Y. Lu, and L.A. Archer, Regulating Li deposition at artificial solid electrolyte interphases, *J. Mater. Chem. A*, 5(2017), No. 7, p. 3483.
[32] D.C. Lin, Y.Y. Liu, W. Chen, *et al*., Conformal lithium fluoride protection layer on three-dimensional lithium by nonhazardous gaseous reagent Freon, *Nano Lett.*, 17(2017), No. 6, p. 3731.
[33] Y. Xu, Y.W. Sun, Y. Sun, H.Y. Fang, Y. Jiang, and B. Zhao, Theoretical calculation study on the electrochemical properties of lithium halide-based artificial SEI films for lithium metal anodes, *Surf. Interfaces*, 44(2024), art. No. 103768.
[34] B. Ouyang, N. Artrith, Z.Y. Lun, *et al*., Effect of fluorination on lithium transport and short-range order in disordered-rocksalt-type lithium-ion battery cathodes, *Adv. Energy Mater.*, 10(2020), No. 10, art. No. 1903240.
[35] Z. Liu, Y. Qi, Y.X. Lin, L. Chen, P. Lu, and L.Q. Chen, Interfacial study on solid electrolyte interphase at Li metal anode: mplication for Li dendrite growth, *J. Electrochem. Soc.*, 163(2016), No. 3, art. No. A592.
[36] M.F. He, R. Guo, G.M. Hobold, H.N. Gao, and B.M. Gallant, The intrinsic behavior of lithium fluoride in solid electrolyte interphases on lithium, *Proc. Natl. Acad. Sci.*, 117(2020), No. 1, p. 73.
[37] L. Chen, K.S. Chen, X.J. Chen, *et al*., Novel ALD chemistry enabled low-temperature synthesis of lithium fluoride coatings for durable lithium anodes, *ACS Appl. Mater. Interfaces*, 10(2018), No. 32, p. 26972.
[38] X.L. Fan, X. Ji, F.D. Han, *et al*., Fluorinated solid electrolyte interphase enables highly reversible solid-state Li metal battery, *Sci. Adv.*, 4(2018), No. 12, art. No. eaau9245.
[39] Y.X. Yuan, F. Wu, G.H. Chen, Y. Bai, and C. Wu, Porous LiF layer fabricated by a facile chemical method toward dendrite-free lithium metal anode, *J. Energy Chem.*, 37(2019), p. 197.
[40] C. Monroe and J. Newman, The impact of elastic deformation on deposition kinetics at lithium/polymer interfaces, *J. Electrochem. Soc.*, 152(2005), No. 2, art. No. A396.
[41] S. Yu, R.D. Schmidt, R. Garcia-Mendez, *et al*., Elastic properties of the solid electrolyte $Li_7La_3Zr_2O_{12}$(LLZO), *Chem. Mater.*, 28(2016), No. 1, p. 197.
[42] J. Ko and Y.S. Yoon, Lithium fluoride layer formed by thermal evaporation for stable lithium metal anode in rechargeable batteries, *Thin Solid Films*, 673(2019), p. 119.
[43] Y.L. Wang, F.M. Liu, G.L. Fan, *et al*., Electroless formation of a fluorinated Li/Na hybrid interphase for robust lithium anodes, *J. Am. Chem. Soc.*, 143(2021), No. 7, p. 2829.
[44] S.F. Liu, X. Ji, J. Yue, *et al*., High interfacial-energy interphase promoting safe lithium metal batteries, *J. Am. Chem. Soc.*, 142(2020), No. 5, p. 2438.
[45] F.A. Soto, P.F. Yan, M.H. Engelhard, *et al*., Tuning the solid electrolyte interphase for selective Li- and Na-ion storage in hard carbon, *Adv. Mater.*, 29(2017), No. 18, art. No. 1606860.
[46] J. Xie, L. Liao, Y.J. Gong, *et al*., Stitching h-BN by atomic layer deposition of LiF as a stable interface for lithium metal anode, *Sci. Adv.*, 3(2017), No. 11, art. No. eaao3170.
[47] X.W. Shen, Y.T. Li, T. Qian, *et al*., Lithium anode stable in air for low-cost fabrication of a dendrite-free lithium battery, *Nat. Commun.*, 10(2019), art. No. 900.
[48] Q. Jin, K.X. Zhao, J.H. Wang, *et al*., Modulating electron conducting properties at lithium anode interfaces for durable lithium–sulfur batteries, *ACS Appl. Mater. Interfaces*, 14(2022), No. 48, p. 53850.
[49] J. Yang, J.M. Hou, Z.X. Fang, *et al*., Simultaneously *in situ* fabrication of lithium fluoride and sulfide enriched artificial solid electrolyte interface facilitates high stable lithium metal anode, *Chem. Eng. J.*, 433(2022), art. No. 133193.
[50] Z.D. Li, L.Y. Huai, S. Li, *et al*., Insight into bulk charge transfer of lithium metal anodes by synergism of nickel seeding and LiF–Li_3N–Li_2S co-doped interphase, *Energy Storage Mater.*, 37(2021), p. 491.
[51] Z. Peng, N. Zhao, Z.G. Zhang, *et al*., Stabilizing Li/electrolyte interface with a transplantable protective layer based on nanoscale LiF domains, *Nano Energy*, 39(2017), p. 662.
[52] X. Ji, S. Hou, P.F. Wang, *et al*., Solid-state electrolyte design for lithium dendrite suppression, *Adv. Mater.*, 32(2020), No. 46, art. No. 2002741.
[53] A.J. Hu, W. Chen, X.C. Du, *et al*., An artificial hybrid interphase for an ultrahigh-rate and practical lithium metal anode, *Energy Environ. Sci.*, 14(2021), No. 7, p. 4115.
[54] J.Y. Wei, X.Q. Zhang, L.P. Hou, *et al*., Shielding polysulfide intermediates by an organosulfur-containing solid electrolyte interphase on the lithium anode in lithium–sulfur batteries, *Adv. Mater.*, 32(2020), No. 37, art. No. 2003012.
[55] Y.P. Sun, Y. Zhao, J.W. Wang, *et al*., A novel organic "polyurea" thin film for ultralong-life lithium–metal anodes via molecular-layer deposition, *Adv. Mater.*, 31(2019), No. 4, art. No. 1806541.
[56] S.X. Deng, Y.P. Sun, X. Li, *et al*., Eliminating the detrimental effects of conductive agents in sulfide-based solid-state batter-

ies, *ACS Energy Lett.*, 5(2020), No. 4, p. 1243.
[57] C. Yan, X.B. Cheng, Y. Tian, *et al*., Dual-layered film protected lithium metal anode to enable dendrite-free lithium deposition, *Adv. Mater.*, 30(2018), No. 25, art. No. 1707629.
[58] R. Xu, X.Q. Zhang, X.B. Cheng, *et al*., Artificial soft-rigid protective layer for dendrite-free lithium metal anode, *Adv. Funct. Mater.*, 28(2018), No. 8, art. No. 1705838.
[59] S.G. Guo, N. Piao, L. Wang, *et al*., PVDF–HFP/LiF composite interfacial film to enhance the stability of Li–metal anodes, *ACS Appl. Energy Mater.*, 3(2020), No. 7, p. 7191.
[60] S.M. Xu, H. Duan, J.L. Shi, *et al.*, *In situ* fluorinated solid electrolyte interphase towards long-life lithium metal anodes, *Nano Res.*, 13(2020), No. 2, p. 430.
[61] C.W. Ma, G. Mu, H.J. Lv, *et al.*, *In situ*-formed flexible three-dimensional honeycomb-like film for a LiF/Li_3N-enriched hybrid organic–inorganic interphase on the Li metal anode, *Mater. Chem. Front.*, 5(2021), No. 13, p. 5082.
[62] C.Y. Fu and C. Battaglia, Polymer–inorganic nanocomposite coating with high ionic conductivity and transference number for a stable lithium metal anode, *ACS Appl. Mater. Interfaces*, 12(2020), No. 37, p. 41620.
[63] S.F. Liu, X.H. Xia, S.J. Deng, *et al.*, *In situ* solid electrolyte interphase from spray quenching on molten Li: A new way to construct high-performance lithium–metal anodes, *Adv. Mater.*, 31(2019), No. 3, art. No. e1806470.
[64] N.W Li, Y.X Yin, C.P Yang, and Y.G Guo, An artificial solid electrolyte interphase layer for stable lithium metal anodes, *Adv. Mater.*, 28(2016), No. 9, p. 1853.
[65] Q.F. Yang, J.L. Hu, J.W. Meng, and C.L. Li, C–F-rich oil drop as a non-expendable fluid interface modifier with low surface energy to stabilize a Li metal anode, *Energy Environ. Sci.*, 14(2021), No. 6, p. 3621.
[66] Y. Gao, Z.F. Yan, J.L. Gray, *et al*., Polymer–inorganic solid–electrolyte interphase for stable lithium metal batteries under lean electrolyte conditions, *Nat. Mater.*, 18(2019), No. 4, p. 384.
[67] C.Z. Zhao, X.Q. Zhang, X.B. Cheng, *et al*., An anion-immobilized composite electrolyte for dendrite-free lithium metal anodes, *Proc. Natl. Acad. Sci.*, 114(2017), No. 42, p. 11069.
[68] S. Wenzel, S. Randau, T. Leichtweiß, *et al*., Direct observation of the interfacial instability of the fast ionic conductor $Li_{10}GeP_2S_{12}$ at the lithium metal anode, *Chem. Mater.*, 28(2016), No. 7, p. 2400.
[69] X.Q. Yu, J.P. Sun, K. Tang, *et al*., Reversible lithium storage in LiF/Ti nanocomposites, *Phys. Chem. Chem. Phys.*, 11(2009), No. 41, art. No. 9497.
[70] J.H. Yan, J.Y. Yu, and B. Ding, Mixed ionic and electronic conductor for Li–metal anode protection, *Adv. Mater.*, 30(2018), No. 7, art. No. 1705105.
[71] J. Maier, Defect chemistry in heterogeneous systems, *Solid State Ionics*, 75(1995), p. 139.
[72] C. Yan, X.B. Cheng, Y.X. Yao, *et al*., An armored mixed conductor interphase on a dendrite-free lithium–metal anode, *Adv. Mater.*, 30(2018), No. 45, art. No. 1804461.
[73] T. Lapp, Ionic conductivity of pure and doped Li_3N, *Solid State Ionics*, 11(1983), No. 2, p. 97.
[74] U.V. Alpen, A. Rabenau, and G.H. Talat, Ionic conductivity in Li_3N single crystals, *Appl. Phys. Lett.*, 30(1977), No. 12, p. 621.
[75] J.R. Li, H. Su, M. Li, *et al*., Fluorinated interface layer with embedded zinc nanoparticles for stable lithium–metal anodes, *ACS Appl. Mater. Interfaces*, 13(2021), No. 15, p. 17690.
[76] P.L. Li, W.L. Feng, X.L. Dong, Y.G. Wang, and Y.Y. Xia, A new strategy of constructing a highly fluorinated solid–electrolyte interface towards high-performance lithium anode, *Adv. Mater. Interfaces*, 7(2020), No. 11, art. No. 2000154.
[77] L.W. Tan, C.L. Wei, Y.C. Zhang, Y.L. An, S.L. Xiong, and J.K. Feng, LiF-rich and self-repairing interface induced by MgF_2 engineered separator enables dendrite-free lithium metal batteries, *Chem. Eng. J.*, 442(2022), art. No. 136243.
[78] W.W. Hou, S.B. Li, J.X. Liang, B. Yuan, and R.Z. Hu, Lithiophilic NiF_2 coating inducing LiF-rich solid electrolyte interphase by a novel NF_3 plasma treatment for highly stable Li metal anode, *Electrochim. Acta*, 402(2022), art. No. 139561.
[79] Z. Peng, J.H. Song, L.Y. Huai, *et al*., Enhanced stability of Li metal anodes by synergetic control of nucleation and the solid electrolyte interphase, *Adv. Energy Mater.*, 9(2019), No. 42, art. No. 1901764.
[80] H.Y. Zhang, S.L. Ju, G.L. Xia, D.L. Sun, and X.B. Yu, Dendrite-free Li–metal anode enabled by dendritic structure, *Adv. Funct. Mater.*, 31(2021), No. 16, art. No. 2009712.
[81] W. Guo, Q. Han, J.R. Jiao, *et al.*, *In situ* construction of robust biphasic surface layers on lithium metal for lithium–sulfide batteries with long cycle life, *Angew. Chem. Int. Ed.*, 60(2021), No. 13, p. 7267.
[82] X.Y. Xu, Y.Y. Liu, J.Y. Hwang, *et al*., Role of Li-ion depletion on electrode surface: Underlying mechanism for electrodeposition behavior of lithium metal anode, *Adv. Energy Mater.*, 10(2020), No. 44, art. No. 2002390.
[83] L.F. Ai, Z.Y. Chen, S.P. Li, *et al*., Stabilizing Li plating by a fluorinated hybrid protective layer, *ACS Appl. Energy Mater.*, 4(2021), No. 12, p. 14407.
[84] L. Gan, K. Wang, Y.Y. Liu, *et al*., Dendrite-free Li-metal anode via a dual-function protective interphase layer for stable Li–metal pouch cell, *Sustain. Mater. Technol.*, 36(2023), art. No. e00585.
[85] A.C. Balazs, T. Emrick, and T.P. Russell, Nanoparticle polymer composites: Where two small worlds meet?, *Science*, 314(2006), No. 5802, p. 1107.
[86] R. Krishnamoorti, Strategies for dispersing nanoparticles in polymers, *MRS Bull.*, 32(2007), No. 4, p. 341.
[87] J.L. Jiang, Y.H. Ou, S.Y. Lu, *et al.*, *In-situ* construction of Li–Mg/LiF conductive layer to achieve an intimate lithium-garnet interface for all-solid-state Li metal battery, *Energy Storage Mater.*, 50(2022), p. 810.
[88] R. Pathak, K. Chen, A. Gurung, *et al*., Fluorinated hybrid solid–electrolyte-interphase for dendrite-free lithium deposition, *Nat. Commun.*, 11(2020), No. 1, art. No. 93.
[89] B.K. Hu, W. Yu, B.Q. Xu, *et al*., An *in situ*-formed mosaic Li_7Sn_3/LiF interface layer for high-rate and long-life garnet-based lithium metal batteries, *ACS Appl. Mater. Interfaces*, 11(2019), No. 38, p. 34939.
[90] H.S. Wang, D.C. Lin, Y.Y. Liu, Y.Z. Li, and Y. Cui, Ultrahigh-current density anodes with interconnected Li metal reservoir through overlithiation of mesoporous AlF_3 framework, *Sci. Adv.*, 3(2017), No. 9, art. No. e1701301.
[91] T.R. Wang, J. Duan, B. Zhang, *et al*., A self-regulated gradient interphase for dendrite-free solid-state Li batteries, *Energy Environ. Sci.*, 15(2022), No. 3, p. 1325.
[92] Z.S. Wang, Z.M. Xu, X.J. Jin, *et al*., Dendrite-free and air-stable lithium metal batteries enabled by electroless plating with aluminum fluoride, *J. Mater. Chem. A*, 8(2020), No. 18, p. 9218.
[93] M.K. Song, J.H. Yim, S.H. Baek, and J.W. Lee, A carbon cloth with a coating layer containing aluminum fluoride as an interlayer for lithium metal batteries, *Appl. Surf. Sci.*, 588(2022), art. No. 152935.
[94] L.L. Wang, S.Y. Fu, T. Zhao, *et al.*, *In situ* formation of a LiF and Li–Al alloy anode protected layer on a Li metal anode with enhanced cycle life, *J. Mater. Chem. A*, 8(2020), No. 3, p. 1247.
[95] F. Li, Y.H. Tan, Y.C. Yin, *et al*., A fluorinated alloy-type interfacial layer enabled by metal fluoride nanoparticle modification for stabilizing Li metal anodes, *Chem. Sci.*, 10(2019), No. 42, p. 9735.